

Interactive comment on “Absorption coefficient of urban aerosol in Nanjing, west Yangtze River Delta of China”
by B. L. Zhuang et al.

by

Anonymous Referee #1

The paper report two years of aerosol absorption coefficient (AAC) measurement in urban Nanjing of China. Data correction of Aethalometer measurement is often overlooked in many existing study in China. It's glad to see that three correction schemes are applied and compared in this study for reporting AAC from Aethalometer measurement. The paper is well written and the measurements are reasonable. The reviewer think the paper can be published on ACP if following comments are addressed.

Dear Reviewer,

Thank you very much for reviewing the manuscript and providing us the constructive comments and suggestions on our study. With respect to your comments, necessary revisions of the paper have been made. We will response to your comments carefully point by point; details of the revisions can be referred to the revised version of the manuscript.

Major comments:

1) Although the annual AAC of 2012 is comparable to 2013, the seasonal distribution of AAC is quite different. Summer AAC in 2012 is higher than 2013, but winter AAC in 2012 is lower than 2013. What's the cause of the different seasonal AAC distribution between two years? Is it associated with meteorology condition or emission?

R: Thank you for your question. High levels of summer AAC in 2012 is associated with the biomass burning in the regions around Nanjing, as discussed in *Zhuang et al. (2014)*. High levels of AAC in winter 2013 might possibly result from large scale regional pollution episodes over East and North China which might be associated with meteorology conditions. Studies on the reasons leading to high BC pollutions (high levels of AAC) in Nanjing during the sampling period (Figure 11) would be carried out and reported in detailed in further publication.

References:

Zhuang, B. L., Wang, T. J., Liu, J., Li, S., Xie, M., Yang, X. Q., Fu, C. B., Sun, J. N., Yin, C. Q., Liao, J. B., Zhu, J. L., and Zhang, Y.: Continuous measurement of black carbon aerosol in urban Nanjing of Yangtze River Delta, China, *Atmos. Environ.*, 89, 415–424, 2014.

2) For the clusters analysis of back trajectories, similar clusters can be grouped together. For example, 2 & 4 in 2012 and 1 & 4 in 2013.

R: Thank you for your suggestion. In our study, recommended clusters were used based on 30 % criterion in Hysplit model. Although some clusters are similar to each other, difference exists. Additionally, AACs and AAEs show different variations to some extent with different

clusters. For example, the transportation speed of air masses in Cluster 4 in 2012 (Figure 8a) is much larger than that in Cluster 2, implying that the source of air masses in Cluster 4 are farther away probably. Hence, aerosols in these air masses have smaller sizes as shown in Figure 9c (Larger AAE values).

The recommended clusters here can provide readers more details and they are reasonable and necessary to some extent.

3) Regarding to the MAE shown in Figure 10a, what instruments are used for absorption coefficient and BC mass concentration measurement respectively? If the BC mass used here is also from Aethalometer, the calculated MAE become circular reference and meaningless.

R: Thank you for your question. BC mass concentration from channel 880 nm of AE-31 has the largest representation of the real BC mass (to minimize the interference from light absorbing organic carbon). Additionally, *Wu et al.* (2009) suggested that linear correlation coefficient between BC from AE-31 at channel 880 nm and BC from Carusso is about 0.97 ($R^2=0.94$) in China, implying that BC mass at channel 880 from AE-31 are reasonable and could be represented real BC mass in the atmosphere to some extent. Thus, BC concentration at channel 880 nm was used to calculate the specific absorption coefficient at 532 nm as following: $MAE_{532nm}=AAC_{532nm \text{ in SC2006}}/BC_{880nm}$, because there were no concomitant or concurrent BC mass measurements by other instruments at our site.

References:

Wu, D., Mao, J. T., Deng, X. J., Tie, X. X., Zhang, Y. H., Zeng, L. M., Li, F., Tan, H. B., Bi, X. Y., Huang, X. Y., Chen, J., and Deng, T.: Black carbon aerosols and their radiative properties in the Pearl River Delta region, *Sci. China Ser. D*, 52, 1152–1163, doi:10.1007/s11430-009-0115-y, 2009.

4) The author conclude that Schmid correction is more reasonable base on the comparison between average AAE from different correction schemes and average AAE retrieved from sun photometer measurement. The referee suggest that a scatter plot between hourly Aethalometer $AAE_{660;470}$ and CE-318 $AAE_{675;440}$ would be more convincing than a single average AAE comparison. The slope and the correlation coefficient can be used to evaluate the degree of agreement between AAE from different correction schemes and AAE from sun photometer.

R: Thank you for your comments. Differences between AAE in SC2006 and the one in WC2003 are derived from the different C values (scattering effects) at different wavelength in these two corrected methods.

C value was set to constant in WC2003 while it was varied with wavelength in SC2006. However, all these values are time-independent, implying that temporal variations of AAE in WC2003 are consistent with the ones in SC2006 although they have different values. And it could be expected that relationship between SC2006-AAE and CE318-AAE is similar to that between WC2003-AAE and CE318-AAE. Therefore, a single average AAE comparison was carried out.

5) Figure 12 can be removed or put in supplemental materials since this information is not

directly associated with the main topic of this paper. The reason of having dynamic cycle time for filter tape advancing in Aethalometer is to avoid overloading of the sampling spot on the filter. When the ATN reach a threshold (adjustable by user in the range of 75 ~ 125), the filter tape will advance to the next position. In other words, when the ambient AAC is higher, ATN takes shorter time to reach threshold. As a result, the interval is shorter when AAC is high. So this phenomenon is just a common characteristic of instrument itself and has nothing to do with the sampling site.

R: Thank you for your suggestion. Fig. 12 will be deleted in revised manuscript. The last paragraph of the Results section (line 12 -22 in Page 19 in discussion typeset manuscript) was deleted, so does Figure 12 in Page 39 in discussion typeset manuscript.

***Interactive comment* on “Absorption coefficient of urban aerosol in Nanjing, west Yangtze River Delta of China” by B. L. Zhuang et al.**

by

Anonymous Referee #3

General Comments: The paper presents 2-year measurements of aerosol absorption optical coefficients at an urban site in Nanjing of China. The paper provides some points to temporal variations of aerosol absorption optical properties and their possible reasons, and influence of biomass burning and pollutions. In fact, high aerosol burden regions such as areas in developing countries are still not well characterized in terms of microphysical and optical changes. The paper also analyzed the influence of meteorological factors on aerosol optical properties. The topic of this paper is of common interest within the scientific community. Although the manuscript includes some important data, however, the quality is not sufficient in the current state to be directly published. The authors should take the suggestions made here into consideration for minor revision.

Dear Reviewer,

Thank you very much for reviewing the manuscript and providing us the constructive comments and suggestions on our study. With respect to your comments, necessary revisions of the paper have been made. We will response to your comments carefully point by point; details of the revisions can be referred to the revised version of the manuscript.

Specific suggestions:

1. In section 2, the authors should add some information of the methods for calculating and correcting aerosol absorptive coefficient, such as WC2003 and SC2006, especially estimating their errors.

R: Thank you very much for your suggestion. Information of the methods for calculating aerosol absorption coefficient has been added to the first paragraph (line 20 in Page 5 in discussion typeset manuscript) of Section 2. Information of the methods for correcting aerosol absorption coefficient has been added to the last paragraph (line 17 in Page 9 in discussion typeset manuscript) of Section 2. Details can be referred to the correction version of the discussion typeset manuscript or revised version of the manuscript.

2. In section 3, the paper gives more analyses of aerosol absorptive coefficient variation and its reasons, however, what is the aim or usefulness of three different methods to calculate and compare coefficients?

R: Thank you for your question. There are several correction methods for the absorption coefficient measured by Aethalometer. The recommended ones used in this study is to figure out the differences in calculating optical properties of absorbing aerosols among different corrections and to understanding the uncertainties in estimating absorption coefficient measured by Aethalometer. Results in this study indeed show that absorption angstrom exponent from WC2003 is much smaller than the one from SC2006 and also smaller than the one from CE-318 as discussed in first paragraph in Section 3.4. The results also show the uncertainties of the absorption coefficient corrected by different methods as listed in Table 1 and discussed in the second paragraph in Section 3.4.

3. More comparison between previous results and this study is needed.

R: Thank you for your suggestion. Comparisons between the relevant works (up to now) and this study has been carried out in Section 3.4 (Line 17-25 in Page 15 and Line 1-3 in Page 16 in discussion typeset manuscript).

4. English needs more revision.

R: Thank you for your suggestion. English correction has been addressed throughout the whole text by Professor J. Liu from University of Toronto, Canada, who is also the co-author of the manuscript.

Change lists

1. The first paragraph (line 20 in Page 5 in discussion typeset manuscript) of Section 2: Add the information of the methods for calculating aerosol absorption coefficient.
2. The last paragraph (line 17 in Page 9 in discussion typeset manuscript) of Section 2: Add information of the methods for correcting aerosol absorption coefficient.
3. Delete Figure 12 and relevant text.

1 **Absorption coefficient of urban aerosol in Nanjing, west Yangtze**
2 **River Delta of China**

3 B. L. Zhuang^{1,4,*}, T. J. Wang^{1,4}, J. Liu^{1,2}, Y. Ma³, C. Q. Yin¹, S. Li^{1,4}, M. Xie^{1,4}, Y.
4 Han^{1,4}, J. L. Zhu¹, X. Q. Yang^{1,4}, C. B. Fu^{1,4}

5 ¹ School of Atmospheric Sciences, Nanjing University, Xianlin Ave. 163, Nanjing 210023, China

6 ² University of Toronto, Toronto M5S 3G3, Canada

7 ³ School of Environmental Science and Engineering, Nanjing University of Information Science and Technology,
8 Ningliu Rd. 219, Nanjing 210044, China

9 ⁴ Collaborative Innovation Center of Climate Change, Jiangsu Province, China

10 * Corresponding author, E-mail: blzhuang@nju.edu.cn; Tel.: +862589681156; fax: +862589683797

11

12 **Abstract:** Absorbing aerosols can significantly modulate shortwave solar radiation in the atmosphere,
13 affecting regional and global climate. Aerosol absorption coefficient (AAC) is an indicator to assess the
14 impact of absorbing aerosols on radiative forcing. In this study, the near-surface AAC and absorption
15 angstrom exponent (AAE) in urban Nanjing, China, are characterized on the basis of measurements in
16 2012 and 2013 using the 7-channel Aethalometer (model AE-31, Magee Scientific, USA). The AAC is
17 estimated with direct and indirect corrections, which show consistent temporal variations and
18 magnitudes of AAC at 532 nm. The mean AAC at 532 nm is about $43.23 \pm 28.13 \text{ Mm}^{-1}$ in urban Nanjing,
19 which is much lower than that in Pearl River Delta and as the same as that in rural areas (Lin'an) in
20 Yangtze River Delta. The AAC in urban Nanjing shows strong seasonality (diurnal variations), high in
21 cold seasons (at rush hours) and low in summer (in afternoon). It also show synoptic and
22 quasi-two-week cycles in response to weather systems. Its frequency distribution follows a typical
23 lognormal pattern. The 532 nm-AAC ranging from 15 to 65 Mm^{-1} dominates, accounting for more than
24 72% of the total data samples in the entire study period. Frequent high pollution episodes, such as those

25 observed in June 2012 and in winter 2013, greatly enhanced AAC and altered its temporal variations
26 and frequency distributions. These episodes are mostly due to local emissions and regional pollutions.
27 Air masses from northern China to Nanjing can sometimes be highly polluted and lead to high AAC at
28 the site. AAE at 660/470 nm from the Schmid correction (Schmid et al., 2006) is about 1.56, which
29 might be more reasonable compared to that from the Weingartner correction (Weingartner et al., 2003).
30 Low AAEs mainly appear in summer in response to the relative humidity (RH). AAC increases with
31 increasing AAE at a fixed aerosol loading. The RH-AAC relationship is more complex. Overall, AAC
32 peaks around RH values of 40% ($1.3 < \text{AAE} < 1.6$), 65% ($\text{AAE} < 1.3$ and $\text{AAE} > 1.6$), and 80%
33 ($1.3 < \text{AAE} < 1.6$).

34

35 **1 Introduction**

36 Atmospheric aerosols, their loadings having increased in recent years, can significant influence
37 regional or global climate because of their direct and indirect interactions with shortwave solar
38 radiation in the atmosphere (Forster et al., 2007). Absorbing aerosols, which is mostly composed of
39 dust in desert areas and of black carbon (BC) in the regions with frequent human activities, can
40 strongly absorb solar radiation, resulting in changes in the atmospheric circulations and hydrological
41 cycle. Although the warming effect of CO₂ could be greatly offset by the scattering aerosol direct effect
42 in the regions with high aerosol concentrations (Kiehl and Briegleb, 1993), it might be further
43 strengthened by BC aerosols because the warming effect of BC aerosols on the global scale is
44 significant, only surpassed by CO₂ (Jacobson 2002). Menon et al. (2002) suggested that the trend of
45 precipitation in China over the past decades, with increased rainfall in the south and drought in the
46 north, might be related to the variation of BC in the region.

47 Previous studies have focused on the aerosol optical properties, radiative forcing and climate
48 effects in both global and regional scales, from model simulations (Penner et al., 2001; Liao and
49 Seinfeld, 2005; Zhuang et al., 2013a; b) and satellite/ground-based observations (Bellouin et al., 2003;
50 Yan et al., 2008; Wu et al., 2012; Zhuang et al., 2014a; etc.) in the past 20 years. Forster et al. (2007)
51 simulated the global mean direct radiative forcing of total aerosols and BC, which ranges between
52 +0.04 and -0.63 W m⁻² and between +0.1 and +0.3 W m⁻², respectively. Over East Asia, the simulated
53 BC direct radiative forcing varies from +0.32 to +0.81 W m⁻² (Zhuang et al., 2013a). All above showed
54 significant uncertainties in estimating the aerosol direct radiative forcing in numerical models. These
55 uncertainties were mostly due to the uncertainties in the aerosol optical properties (Holler et al., 2003)
56 which were related to the aerosol emissions, profiles, compositions and mixing states. Forster et al.
57 (2007) stated that the uncertainties could be reduced if observed aerosol optical properties were
58 employed when estimating the forcing. China has experienced rapid population and economic growth
59 during the past three decades, resulting in enhanced aerosol and trace gas emissions. Streets et al. (2001)
60 suggested that the BC emissions in China roughly accounts for one-fourth of the global anthropogenic
61 emissions, although the uncertainty about this estimate is large. The BC aerosols are mostly emitted in
62 Southwest, North China, Yangtze River Delta (YRD) and Pearl River Delta (PRD) regions (Zhang et al.,
63 2009). Recently, many observation-based studies are conducted on the aerosol optical properties and
64 direct radiative forcing over China (Xu et al., 2004; Yan, 2006; Xia et al., 2007; Yan et al., 2008; He et
65 al., 2009; Wang et al., 2009; Wu et al., 2009; Li et al., 2010; Cai et al., 2011; Bai et al., 2011; Xiao et al.,
66 2011; Zhou et al., 2011; Wu et al., 2012; etc.). Some of them focused on the total extinction or optical
67 depth of the aerosols. Xia et al. (2007) reported that the annual mean optical depth (AOD) at 500 nm
68 and Angstrom exponent (AE) of total aerosols in YRD were 0.77 and 1.17, respectively. Xiao et al.

69 (2011) analyzed the temporal and spatial variations of the total aerosol optical depth and Angstrom
70 exponent using CE-318 in Hangzhou. Zhuang et al. (2014a) suggested that column AOD and AE of
71 absorbing aerosols were 0.04 ± 0.02 and 1.44 ± 0.50 in urban Nanjing. The aerosol absorption coefficients
72 (AAC) were also studied for several urban and rural areas of China. AAC at 565 nm in Gobi desert was
73 found to be as low as $6 \pm 11 \text{ Mm}^{-1}$ (Yulin) (Xu et al. 2004). The annual 532 nm-AAC was about 17.54
74 $\pm 13.44 \text{ Mm}^{-1}$ at a rural site while it was about $45 \pm 39 \text{ Mm}^{-1}$ at an urban site, in Beijing (Yan et al.
75 2008; He et al. 2009). AAC at 532 nm was as large as $82 \pm 23 \text{ Mm}^{-1}$ at urban areas of Pearl River Delta
76 (PRD) in South China (Wu et al. 2009).

77 Although considerable researches on this issue have been performed, it's still insufficient in
78 regional scale in China and there is a lack of study on AAC in YRD, one of the fastest growing regions
79 in China. Therefore, this study is to address this issue by characterizing AAC in the region using the
80 near-surface absorption coefficient and Angstrom exponent of absorbing aerosols in urban Nanjing, a
81 typical developing city in west Yangtze River Delta of China. The method is described in Section 2.
82 Results and discussions are presented in Section 3, followed by Conclusions in Section 4.

83

84 **2 Methodologies**

85 **2.1 Sampling station and instruments**

86 Sampling site is located in the Gulou campus of Nanjing University, urban Nanjing (32.05° N ,
87 118.78° E). It is built on the roof of a 79.3 m-tall building, around which there are no industrial
88 pollution sources within a 30 km radius but there are several main roads with apparent traffic pollution.
89 The sketch map of the site (not shown) can be referred to Figure 1 of Zhu et al. (2012). The black
90 carbon aerosol mass concentration and aerosol absorption coefficient were derived from the

91 measurements using the 7-channel Aethalometer (model AE-31, Magee Scientific, USA). The AE-31
92 model measures light attenuation at seven wavelengths (370, 470, 520, 590, 660, 880, and 950 nm,
93 respectively). The aerosol inlet is located ~1 m above the roof. Routine flow calibration and blank tests
94 were performed before sampling. Details on the AE-31 and its sampling principles can be referred to
95 Hansen et al. (1984), Weingartner et al. (2003) and Arnott et al. (2005). Near-real-time continuous
96 measurements were made at the site since 1 January 2012, using the AE-31, with a desired flow rate of
97 5.0 L/min and a sampling interval of 5 min. Two-year's data in 2012 and 2013 are used in this study.
98 Meteorological data are from the National Meteorological Station of Nanjing (No. 58238).

99

100 2.2 Calculation of AE-31_absorption coefficient

101 The absorption coefficient is defined with Beer-Lambert's law as shown in Eq. 1
102 in Weingartner et al. (2003) and Arnott et al. (2005), which is associated with the intensities of the
103 incoming light and remaining light after passing through a medium. A variable ATN, which is
104 given as percentage value, is defined to represent filter attenuation through the sample spot in the
105 tape (Eq. 2 in Weingartner et al., 2003 and Arnott et al., 2005) inside the instrument. Aerosol light
106 absorption coefficient and BC mass concentration can be calculated directly based on the
107 measured light attenuation through a quartz filter matrix. There are two ways in calculating
108 aerosol light absorption coefficient. Aerosol light absorption coefficient can be calculated directly or
109 ~~indirectly.~~The indirect calculation (IDC for short), which is much simpler than the direct ones, is
110 expressed as Eq. 1.

$$111 \quad \sigma_{\text{abs},f}(\lambda) = [BC] \times \gamma \quad (1)$$

112 where, [BC] is the mass concentration of Aethalometer BC (in $\mu\text{g}/\text{m}^3$) without any correction and γ

113 is the conversion factor determined empirically from linear regression of the Aethalometer BC
 114 concentration versus the aerosol absorption measurement (Yan et al., 2008). Wu et al. (2009) indicated
 115 that the conversion factor γ from the linear regression of the Aethalometer BC concentrations (ng/m³)
 116 at 880 nm against the light absorption coefficient (Mm⁻¹) at 532 nm in South China was about 8.28
 117 m²/g. $\gamma=11.05$ m²/g in the suburb of Nanjing.

118 In addition to the indirect way, wavelength-depended aerosol absorption coefficient can be
 119 calculated directly based on the measured light attenuation (ATN) at seven wavelengths (370, 440, 520,
 120 590, 660, 880 and 950 nm) as shown in Eq. 2:

$$121 \quad \sigma_{\text{ATN},t}(\lambda) = \frac{(\text{ATN}_t(\lambda) - \text{ATN}_{t-1}(\lambda))}{\Delta t} \times \frac{A}{V} \quad (2)$$

122 where, A (in m²) is the area of the aerosol-laden filter spot, V is the volumetric sampling flow rate
 123 (in L/min) and Δt is the time interval (=5 min) between t and $t-1$. It is well known that σ_{ATN}
 124 is generally larger than the actual aerosol absorption coefficient σ_{abs} because of the optical
 125 interactions of the filter substrate with the deposited aerosol (Petzold et al., 1997; Weingartner et al.,
 126 2003; Arnott et al., 2005; Schmid et al., 2006). The key factors leading to the bias include: 1) multiple
 127 scattering of light at the filter fibers (multiple scattering effect), which may result in the overestimation
 128 of the σ , and 2) instrumental response with increased particle loading on the filter (shadowing effect),
 129 which may lead to underestimation of the σ . Therefore, the calibration factors C and R (shown in Eq.
 130 3) are introduced to address the scattering effect and shadowing effect, respectively:

$$131 \quad \sigma_{\text{abs},t}(\lambda) = \frac{\sigma_{\text{ATN},t}(\lambda)}{C \times R} \quad (3)$$

132 To address the uncertainties, several correction algorithms, including Weingartner (Weingartner et
 133 al., 2003), Arnott (Arnott et al., 2005), Schmid (Schmid et al., 2006), Virkkula (Virkkula et al., 2007)
 134 corrections, have been developed. Collaud Coen et al. (2010) suggested that both Weingartner

135 (WC2003 for short, hereinafter) and Schmid (SC2006 for short, hereinafter) corrected-absorptions have
 136 good agreements with the one from Multi-Angle Absorption Photometer. Therefore, these two
 137 corrections, which have similar formula shown in Eq. 4, are applied in this study to investigate the
 138 absorption coefficient:

$$139 \quad \sigma_{\text{abs},t}(\lambda) = \frac{\sigma_{\text{ATN},t}(\lambda)}{C \times \left(\left(\frac{1}{f} - 1 \right) \times \frac{\ln(\text{ATN}_t(\lambda)) - \ln 10}{\ln 50 - \ln 10} + 1 \right)} \quad (4)$$

140 Both of them have the same $R(\lambda)$:

$$141 \quad R_t(\lambda) = \left(\frac{1}{f} - 1 \right) \times \frac{\ln(\text{ATN}_t(\lambda)) - \ln 10}{\ln 50 - \ln 10} + 1 \quad (5)$$

142 And $R=1$ when $\text{ATN} \leq 10$. f can be calculated according to [Weingartner et al. \(2003\)](#):

$$143 \quad f(\lambda) = n \times (1 - \omega(\lambda)) + 1 \quad (6)$$

144 Where ω is the wavelength depended single scattering albedo (SSA) and n is a constant
 145 ($=0.86 \pm 0.01$). Note that the reliability of n value (0.86) is limited because this value is mostly
 146 estimated under the condition of $\omega < 0.6$, which may result in large bias. Therefore, an empirical
 147 $f=1.2$ (when $\omega \approx 0.9$), which is independent of wavelength as suggested by [Schmid et al. \(2006\)](#), is
 148 used for both WC2003 and SC2006 in this study.

149 The multiple-scattering correction in WC2003 is also different from that in SC2006. Weingartner
 150 ([Weingartner et al., 2003](#)) indicated that the two waveband (450 and 660 nm) averaged C was about
 151 3.6 for non-fresh soot. In this study, C in WC2003 is independent of wavelength and is set 3.48 for
 152 China according to [Wu et al. \(2013\)](#). In contrast, Schmid ([Schmid et al., 2006](#)) pointed out that C ,
 153 which is wavelength depended, is initially expressed as following:

$$154 \quad C(\lambda) = C^*(\lambda) + m_s(\lambda) \times \frac{\omega(\lambda)}{1 - \omega(\lambda)} \quad (7)$$

155 where m_s represents the fraction of the aerosol scattering coefficient and ω is SSA. Optical
 156 properties from CE-318 were used in this study because there was no concomitant scattering
 157 measurements at the site during the whole sampling period. Thus, we assumed that SSA and Angstrom
 158 exponent (AE) at the low layers of atmosphere were equated to the column ones. According to [Zhuang](#)
 159 [et al. \(2014a\)](#), annual mean $\omega(440)=0.922$, $\omega(675)=0.924$, and $\alpha_{a,675/440nm}=1.44$ at the site.

160 Based on $\alpha_{a,675/440nm}$ and according to the definition:

$$161 \quad \omega(\lambda) = \frac{\sigma_s(\lambda)}{\sigma_s(\lambda) + \sigma_a(\lambda)} \quad (8)$$

162 $\alpha_{s,675/440nm}$ can be calculated as the following ([Angstrom. 1929](#)):

$$163 \quad \alpha_{s,675/440nm} = -\frac{\log\left(\frac{\sigma_s(675)}{\sigma_s(440)}\right)}{\log(675/440)} = -\frac{\log\left(\frac{1-\omega(440)}{\omega(440)} \times \frac{\omega(675)}{1-\omega(675)}\right)}{\log(675/440)} + \alpha_{a,675/440nm} \quad (9)$$

164 Thus, $\alpha_{s,675/440nm}=1.51$.

165 All wavelength-depend SSAs could be calculated based on the following formula ([Schmid et al.,](#)
 166 [2006](#)):

$$167 \quad \omega(\lambda) = \frac{\omega_0 \times \left(\frac{\lambda}{\lambda_0}\right)^{-\alpha_s}}{\omega_0 \times \left(\frac{\lambda}{\lambda_0}\right)^{-\alpha_s} + (1-\omega_0) \times \left(\frac{\lambda}{\lambda_0}\right)^{-\alpha_a}} \quad (10)$$

168 Here, ω_0 , λ_0 , and $\alpha_{s,675/440}$ were set to 0.922, 440 nm and 1.51, respectively. Based on the given

169 $C^*(\lambda)$ and $m_s(\lambda)$ in Table 1 of [Arnott et al. \(2005\)](#), $C(\lambda)$ of pure candle light soot was

170 estimated. To parameterize the dependence among $C(\lambda)$, λ and α_a , $\ln(C)$ versus $\ln(\lambda)$ for

171 $\alpha_a=1, 1.5, 2$ and 2.5 were plotted in Figure 1 and a quadratic fit (universal formula as shown in Eq. 11)

172 for each α_a value was made following Schmid ([Schmid et al., 2006](#)) who suggested that the fits in

173 Figure 1 were applicable to other kind of soot based on given ω and α_s .

174 $\ln(C(\lambda)) = A \times \ln(\lambda)^2 + B \times \ln(\lambda) + D$ (11)

175 Eq. 11 can be transformed into:

176
$$C(\lambda) = C_{ref} \times \frac{\lambda^{A \times \ln(\lambda) + B}}{\lambda_{ref}^{A \times \ln(\lambda) + B}}$$
 (12)

177

178 α_a -dependent A and B are shown in the quadratic equations of Figure 1. A and B versus α_a

179 are shown in Figure 2 and a quadratic fit is made based on the given ω and α_s at our site for A

180 and B individually shown as Eq. 13 and Eq. 14.

181
$$A = 0.123 \times \alpha_a^2 - 0.128 \times \alpha_a - 0.195$$
 (13)

182
$$B = -1.512 \times \alpha_a^2 + 1.774 \times \alpha_a + 2.637$$
 (14)

183

184 Based on Eq. 12, 13 and 14, $C(\lambda)$ at our site could be estimated for a given α_a and C_{ref} .

185 Schmid et al. (2006) indicated that C_{ref} at 532 nm is about 2.1 and 4.0 for pure or external mixtures

186 of soot and internal mixtures of soot, respectively. For the urban aerosols, the mean value 3.6 (Schmid

187 et al., 2006) was suggested and used in this study. Thus C was 2.95, 3.37, 3.56, 3.79, 3.99, 4.51 and

188 4.64 at 370, 470, 520, 590, 660, 880, and 950 nm, respectively.

189 As indicated in Coen et al. (2010), Virkkula correction and Arnott correction are not recommended
 190 to be used to correct the absorption coefficient because the Virkkula correction does not consider all the
 191 known artifacts and Arnott correction has technical limits due to the generation of new negative
 192 absorption coefficient values. Although the determination of the f constant used in the WC2003 is not
 193 clearly defined, it still shows a very good agreement with the Multi-Angle Absorption Photometer.
 194 Similar to Arnott correction, SC2006 also introduces artifacts in the absorption wavelength dependence,
 195 but to a lesser extent. And it also shows a very good agreement with the Multi-Angle Absorption

196 [Photometer \(Coen et al., 2010\)](#). Therefore, to estimate absorption coefficient of the aerosol in
 197 urban Nanjing, both direct and indirect ways introduced above were employed in this study although
 198 the indirect way could only address σ_{abs} at 532 nm. To make the comparison, 532 nm- σ_{abs} from
 199 WC2003 and SC2006 was derived using the 520 and 590 nm- σ_{abs} according the following equations
 200 (Angstrom, 1929):

$$201 \quad \alpha_{abs,590/520nm} = -\frac{\log(\sigma_{abs,590nm} / \sigma_{abs,520nm})}{\log(590_{nm} / 520_{nm})} \quad (15)$$

$$202 \quad \sigma_{abs,532nm} = \sigma_{abs,520nm} \times \left(\frac{532_{nm}}{520_{nm}}\right)^{-\alpha_{abs,590/520nm}} \quad (16)$$

203

204 **3 Results and discussions**

205 **3.1 Temporal variations of the aerosol absorption coefficient**

206 We corrected the aerosol absorption coefficient (AAC) using three methods: an indirect correction
 207 (IDC), [Weingartner et al. \(2003\)](#) (WC2003) and [Schmid et al. \(2006\)](#) (SC2006), in urban Nanjing
 208 during the period from 2012 to 2013. It is worth noting that the indirect correction could only estimate
 209 a single wavelength AAC (at 532 nm). To make it comparable, 532 nm-AACs from WC2003 and
 210 SC2006 were calculated by Eq. 15 and Eq. 16. Temporal variations of AACs for the rest of
 211 wavelengths from WC2003 and SC2006 corrections are similar to those of 532 nm-AAC (not shown).

212 Figure 3 presents the monthly variations of 532 nm-AAC in urban Nanjing in 2012 (Figure 3a)
 213 and 2013 (Figure 3b) corrected by IDC, WC2003 and SC2006. The seasonal variations and the
 214 magnitude of AAC at 532 nm agree closely between the direct and indirect corrections. The relatively
 215 large difference in AACs between the direct and indirect corrections was in spring and summer (wet
 216 seasons) both in 2012 and 2013. The difference is mostly caused by the shadowing effect R because

217 [BC] directly from AE-31 in Eq. 1 has not been corrected. The bias of the actual BC concentration from
218 [BC] is from the R as suggested by Eq.7 in Schmid et al. (2006) and Eq. 7 in Weingartner et al. (2003).
219 Thus, the results imply the importance of the shadowing effect in estimating AACs. The 2-year mean of
220 AAC at 532 nm averaged from the three corrections is about $43.23 \pm 28.13 \text{ Mm}^{-1}$, with a maximum and
221 a minimum of 273 Mm^{-1} and 1.28 Mm^{-1} , respectively, in urban Nanjing. AAC at 532 nm corrected by
222 IDC is the largest (44.38 Mm^{-1}), followed by that from WC2003 (43.38 Mm^{-1}) and SC2006 (41.93
223 Mm^{-1}). AACs in 2012 were a little smaller than those in 2013. The AAC in urban Nanjing has an
224 evident seasonal variation in both 2012 and 2013, generally higher in cold seasons and mostly lower in
225 warm seasons. Both precipitations and BC emissions may influence the seasonal variations in the AAC
226 to some extent. In summer, high frequent precipitation and low BC emissions (Zhang et al., 2009)
227 result in low BC concentrations, which is opposite to those in winter as suggested by Zhuang et al.
228 (2014b). Additionally, serious pollution episodes would lead to high levels of BC loadings, thus
229 considerably enhancing AACs. Although AACs are generally expected to be small in summer due to
230 low BC concentrations, AAC in June 2012 was substantially large (Fig. 3a). The monthly mean AAC
231 from SC2006 in this month is 51.89 M m^{-1} , which is about 1.5, 1.4 and 1.8 times to that in June in 2012,
232 in summer of 2012 and 2013, respectively. Such high AAC value is mainly resulted from a seriously
233 polluted event of BC during the period from 1st to 15th of June 2012. High BC loadings during this
234 period were due to a high intensity of biomass burning in northwestern region of Nanjing (Zhuang et al.
235 2014b). Fig. 3 shows that the monthly variation of AAC in 2012 was different from that in 2013. The
236 highest values of AAC were in June and October 2012 while in 2013, AAC was at the maximum in
237 winter (January, November and December). The large differences between the two years may be due to
238 the difference in pollution episodes, which eventually results in different seasonal variations of AACs

239 in Fig. 3.

240

241 AAC also has substantial diurnal variations (Figure 4). Its levels are high at rush hours (around 7-9
242 o'clock am and pm) but low in afternoon (around 1-3 o'clock pm) almost in all seasons in urban
243 Nanjing in 2012 and 2013. At 7 o'clock am, averaged 532 nm-AAC was as large as about 50 Mm^{-1} ,
244 while at 2 o'clock pm, it was about 33 Mm^{-1} . Normally, large AACs during these periods of the day
245 might be caused by the vehicle emissions (because the site is surround by several main roads with
246 apparent traffic pollution as mentioned in Section 2) while the small AACs in afternoon was induced by
247 well developed boundary layer (Zhuang et al. 2014b). Because the diurnal variations of AAC at 532 nm
248 from IDC, WC2003 and SC2006 are similar (Fig 4a), one of them (SC2006) was selected to
249 characterize the AAC's diurnal variation in detail (Fig. 4b). AAC's diurnal variation shows much
250 stronger seasonality in 2013 than that in 2012 (Fig. 4b), which might be caused by substantial pollution
251 episodes discussed above. In 2012, highly intensified biomass burning in early June near Nanjing
252 resulted in a higher BC level (Zhuang et al., 2014b) and thus a larger AAC than those in 2013.
253 Extremely high levels of AAC in winter in 2013 might also result from the poor air quality during these
254 periods. In addition to its seasonality, the diurnal cycle itself could deviate from its normal pattern
255 (peak at rush hours and trough in afternoon). Fig. 4b also shows that the standard deviations of AAC in
256 2012 (25.12 Mm^{-1}) are smaller than those in 2013 (28.58 Mm^{-1}) although their averaged values in 2012
257 and 2013 are closed to each other.

258

259 **3.2 Frequencies of the aerosol absorption coefficient**

260 Similar to the seasonal variations, the frequency patterns of AACs for the rest of wavelengths are

261 consistent to those of 532 nm-AAC so the discussion is focused on the frequency of 532 nm-AAC only
262 to avoid duplication. Figure 5a shows the frequency distributions of 532 nm-AAC corrected by IDC,
263 WC2003 and SC2006 during the entire study period, which followed typical lognormal patterns. The
264 range from 15 to 65 Mm^{-1} dominated, accounting for more than 72% of the total data samples during
265 the entire period. The maximum frequencies of 10.07% (IDC), 10.57% (WC2003), and 10.89%
266 (SC2006) occurred at the ranges from 25 to 30 Mm^{-1} . The absolute differences between the directly and
267 indirectly corrected AACs are relatively larger at the range from 20 to 25 Mm^{-1} than those in other
268 ranges, possibly due to the influence of the shadowing effect in warming seasons as analyzed in
269 Section 3.1. Because of the consistency of the frequency patterns and order of magnitudes among the
270 three AACs, only the frequency of SC2006 AAC at 532 nm is presented in detail, illustrating the
271 inter-annual and seasonal variations of the frequency (Fig. 5b and Fig. 5c). Similar to the diurnal cycles,
272 frequency distributions of AAC in 2012 are more consistent with each other and more concentrated
273 than those in 2013. Frequencies at the ranges below 25 Mm^{-1} (28.57%) and above 70 Mm^{-1} (10.62%)
274 are smaller in 2012 compared to 2013 (31.09% and 15.47%, respectively). The peak frequency mostly
275 occurs at the smaller AAC range in summer while at the larger ones in other seasons. Additionally,
276 pollution episodes might alter the shape of the frequencies especially on seasonal or monthly scales.
277 High levels of aerosol loadings and its AACs would be observed during the period of the episodes,
278 which might lead to relatively higher frequency occurred at the larger AAC ranges. As shown in Fig. 5c,
279 frequencies of the values exceeding 65 Mm^{-1} were larger in fall compared to those in other seasons in
280 2012. Frequencies of the values larger than 55 Mm^{-1} were higher in winter compared to those in other
281 seasons in 2013. In summer 2012, frequencies of AAC ranging from 120 to 140 Mm^{-1} was larger
282 (0.94%) than those in spring (0.65%) and winter (0.58%) due to the biomass burning in northwestern

283 regions of Nanjing ([Zhuang et al., 2014b](#)). Over all, frequencies of AAC in 2013 show much more
284 seasonality compared to 2012. Large differences of the frequency distribution between 2012 and 2013
285 are mainly found in summer and winter.

286

287 **3.3 Periodic variation of the aerosol absorption coefficient**

288 In addition to diurnal cycles, AAC in Nanjing might have other periodicities during the study
289 period. Thus, Morlet wavelet is employed based on daily mean values of AAC at 532 nm corrected by
290 SC2006. Figure 6 shows the wavelet power spectrum (Figure 6a) and wavelet real part spectrum
291 (Figure 6b) of 532 nm-AAC. Cycles of 4-8 days and 9-17 days which are mostly statistically
292 significant at the confidence level of 95% dominate the local power spectrum, implying that variations
293 of AAC in urban Nanjing could also be affected by synoptic scale (weekly) weather systems and
294 quasi-two-week scale systems to some extent. The oscillations of AAC on the synoptic scale are found
295 in the period from late fall to early winter due to the quick and vigorous weather change. And
296 quasi-two-week scale oscillations of AAC are mainly in winter. Similar to AAC, visibility in Nanjing
297 also has synoptic scale and quasi-two-week scale periodic variations as indicated in [Deng et al. \(2011\)](#),
298 who suggested that the quasi-two-week oscillation might be a regional rather than local phenomenon in
299 China even in East Asia.

300

301 **3.4 Varied with wavelength of the aerosol absorption coefficient**

302 In the previous sections, single wavelength AAC (at 532 nm) is discussed as the AAC
303 distributions and seasonal variations are similar among different wavelengths. In this section,
304 wavelength depended AACs as well as absorption angstrom exponents (AAE) at 660/470 nm corrected

305 by WC2003 and SC2006 are further examined (Fig. 7). AACs from both WC2003 and SC2006
306 decrease with increasing wavelength (Fig. 7a). Although AAC at 532 nm from WC2003 is closed to
307 that from SC2006, substantial differences exist at other wavelengths. WC2003-AACs are smaller than
308 SC2006-AACs at shorter wavelengths (370 and 470 nm) but are larger than SC2006-ACCs in longer
309 wavelengths (from 590 nm to 950 nm). The averaged AACs range from 23.40 (at 950 nm) to 68.89
310 Mm^{-1} (at 370 nm) based on WC2003 and range from 17.56 (at 950 nm) to 82.07 Mm^{-1} (at 370 nm)
311 based on SC2006. Different correction methods on scattering effect C between WC2003 and SC2006
312 result in different variations of AAC with wavelengths because C in WC2003 is independent of
313 wavelength, and subsequently might lead to considerably different AAEs between these corrections
314 (Fig. 7b and 7c). Both Fig. 7b and 7c show that AAE at 660/470 nm from SC2006 is much larger than
315 that from WC2003, although they have similar seasonal variations. Annual mean 660/470 nm AAEs in
316 2012 and 2013 are 1.58 and 1.54 from SC2006 and 1.09 and 1.07 from WC2003. AAE from SC2006 is
317 about 1.5 times to that from WC2003. Additionally, AAE has strong seasonality with the high level in
318 winter and low level in summer, implying that absorbing aerosols in summer have larger sizes possibly
319 caused by large relative humidity (RH). Seasonal variations of AAE from AE-31 are similar to those
320 from CE-318 as compared with those in [Zhuang et al. \(2014a\)](#), who reported annual mean AAE of the
321 column aerosols from CE-318 being 1.44 at the site. Thus, this suggests that the scattering correction
322 method by [Schmid et al. \(2006\)](#) were more reasonable than that by [Weingartner et al. \(2003\)](#).

323

324 Table 1 summaries the optical properties of absorbing aerosols from AE-31 based on IDC,
325 WC2003 and SC2006. Two-years averaged values of AAC at 532 nm corrected by these three methods
326 are 44.38, 43.38 and 41.93 Mm^{-1} , respectively, in urban Nanjing. 660/470 nm AAE corrected by

327 WC2003 and SC2006 are 1.08 ± 0.20 and 1.56 ± 0.23 , respectively. Annual mean AAC averaged from
328 all wavelengths is 40.78 Mm^{-1} (SC2006) and 41.41 Mm^{-1} (WC2003), while it is 41.47 Mm^{-1} (SC2006)
329 $\sim 42.97 \text{ Mm}^{-1}$ (WC2006), averaged from visible wavelengths. The inter-annual difference suggests that
330 AAC in 2012 is smaller than that in 2013, while AAE in 2012 is larger than that in 2013. The scattering
331 correction of [Weingartner et al. \(2003\)](#) is different from that of [Schmid et al. \(2006\)](#), which would
332 result in large variances of AAC at shorter ($<520 \text{ nm}$) or longer ($>590 \text{ nm}$) wavelengths, causing large
333 difference of AAE between the two methods. However, AACs at 532 nm or averaged from all
334 wavelengths from WC2003 and SC2006 are closed to each other. Many studies on aerosol optical
335 properties have been carried out by model simulations and observations. Most of them focused on the
336 optical depth and single scattering albedo of column (from surface to the top of the atmosphere)
337 aerosols ([Zhuang et al., 2014a](#)), few on the aerosol absorption coefficient, even less on AAC in urban
338 areas of YRD. Annual AAE at $660/470 \text{ nm}$ corrected by SC2006 agree well with the one observed by
339 CE-318 at the site. [Xu et al. \(2004\)](#) pointed out that AAC at 565 nm was $6 \pm 11 \text{ Mm}^{-1}$ in Gobi desert
340 (Yulin) in China in 1999. In Beijing, capital of China, annual AAC at 532 nm was about 17.54 ± 13.44
341 Mm^{-1} at a rural site (Shangdianzi: SDZ) in 2003 and 2004 ([Yan et al., 2008](#)) while it was about 45 ± 39
342 Mm^{-1} at an urban site from 2005 to 2006 ([He et al., 2009](#)). AAC at 532 nm at rural site of YRD (Lin'an)
343 was about $44.3 \pm 19.7 \text{ Mm}^{-1}$ in 2004 ([Yan, 2006](#)). In the semi-arid area in Northeast China (Tongyu),
344 AAC at 520 nm was only about $7.28 \pm 5.87 \text{ Mm}^{-1}$ from 2010 to 2011 ([Wu et al., 2012](#)). In Pearl River
345 Delta (PRD) of China, annual AAC at 532 nm was as large as $82 \pm 23 \text{ Mm}^{-1}$ at urban areas from 2004
346 to 2007 ([Wu et al., 2009](#)). Levels of annual AAC in urban Nanjing, to some extent, were comparable to
347 those in other Chinese urban or rural sites. Comparisons suggest that AAC in urban Nanjing (YRD)
348 were much lower than those in PRD but higher than those in non-urban sites of North China

349 (Shangdianzi, Tongyu and Yulin). In YRD, annual AAC in urban Nanjing was as large as that in rural
350 areas (Lin'an), which is similar to the BC concentrations there (Zhuang et al., 2014b).

351

352 **3.5 Aerosol absorption coefficient in different wind directions**

353 In addition to local emissions, the meteorological factors such as the prevailing wind could also
354 affect the AAC and AAE in urban Nanjing. Backward trajectories analysis shown in Fig. 8a and 8b
355 indicated that Nanjing could be affected by local air flow and long-distance air flows mostly from
356 northwestern, northern, eastern, southeastern and southern direction both in 2012 and 2013, implying
357 that the prevailing winds might have weaker inter-annual variations compared to the aerosols. Air flows
358 from northern directions account for about the half of the totals while the local air flow and the flows
359 from the oceans account for about 13%, ~19% and 15%, respectively. Frequencies of air flows from
360 south and northwest China are relatively smaller. Rose plot of near surface wind around the site (32° N,
361 118.76° E, 8 m tall) during the entire study period (Fig. 8c) suggests that the distributions of the near
362 surface wind directions somewhat agree with those from the backward trajectory analysis. However,
363 the winds near the surface come from the southeastern to eastern directions more frequently,
364 accounting for more than 35% of the totals. Probabilities of the wind from south to west account for the
365 least (Fig. 8c). The wind speed is mostly concentrated in the values from 2 to 6 m/s in Nanjing during
366 the period.

367

368 As mentioned above, wind direction shifting over different seasons might be another important
369 factor in determining the aerosol AAC and AAE. Zhuang et al. (2014b) indicated that high BC loadings
370 in fall and summer of 2012 were observed at the site when winds were from northeastern and

371 northwestern directions, in which air masses might be highly polluted, thus leading to considerably
372 large AAC. Figure 9 presents the levels of AAC at 532 nm and AAE at 660/470 nm corrected by
373 SC2006 associated with different clusters (shown in Figure 8) in urban Nanjing both in 2012 and 2013.
374 Considerable air pollutants are derived from local and sub-regional emissions as presented in cluster 6
375 (Fig. 9a and 8a) in 2012 and in cluster 3 (Fig. 9b and 8b) in 2013, with averaged values of 56.13 Mm^{-1}
376 and 65.38 Mm^{-1} , respectively. Air masses from the oceans and south China (sea) (cluster 7, 8 and 9 in
377 Fig. 8a and 8b) were relatively clean, leading to smaller AACs in Nanjing (Fig. 9a and 9b), with
378 averaged values of 33.28 Mm^{-1} in 2012 and 30.1 Mm^{-1} in 2013. The air masses from the remote sites
379 (cluster 2, 3 and 4 in 2012 in Fig. 8a and cluster 1, 4 and 5 in 2013 in Fig. 8b) could also bring the
380 clean air and then might result in relatively low levels of AACs in Nanjing. Previous analysis indicates
381 that prevailing winds have weak inter-annual variations. Thus, substantial differences (about 15 Mm^{-1})
382 between AAC from cluster 3 (or cluster 5) in 2012 and cluster 2 (or cluster 6) in 2013 might mostly
383 result from the regional pollution episodes in North China in 2013. In addition to AAC, AAE levels are
384 also somewhat affected by different air flows. Fig. 9c and 9d suggest that AAE in urban Nanjing is
385 relatively small when the air masses come from the oceans (cluster 7 and 9) possibly due to the
386 affection of moisture while is larger when the flows are from the areas of higher latitudes. Local AAEs
387 are 1.52 (in cluster 6 in Fig. 9c) in 2012 and 1.62 (in cluster 3 in Fig. 9d) in 2013, which are closed to
388 the annual mean value of 1.56.

389

390 **3.6 Relationship between aerosol absorption coefficient and its absorption angstrom exponent**

391 Aerosol absorption coefficient is directly determined by the loadings of absorbing aerosols.

392 Additionally, both aerosol size's distribution and relative humidity (RH), especially the former, are

393 closely related to the variation in AAC. Figure 10 shows the relationships among AAC at 532 nm
394 corrected by SC2006, AAE at 660/470 nm corrected by SC2006 and RH. It suggests that changes in
395 aerosol mass (or specific) absorption coefficients (MAC for short, defined as ratios of AAC to BC
396 loading, in m^2/g) at 532 nm are closely relative to the variations of AAE. High levels of MAC mostly
397 appear in the ranges with large AAE, implying that absorbing aerosols with smaller sizes might absorb
398 more solar radiation because the fine particles have much larger specific surface areas compared to
399 coarse ones. The linear correlation coefficient between MAC and AAE exceeds 0.92 in urban Nanjing
400 during the study period (Fig. 10a). Changes in AAE somewhat are influenced by the variations of RH.
401 Fig. 10a also indicates that large AAEs are mostly found when the RH is low and vice versa. Generally,
402 moist air is in favor of hygroscopic growth of the aerosols, thus resulting in smaller AAE
403 (corresponding to large size of the aerosols). These results could further explain why AAE in urban
404 Nanjing is relatively small when the air masses come from the oceans as discussed in the previous
405 section (Fig. 8 and 9). In addition to AAE, AAC is also affected by RH, as shown in Fig. 10b for
406 AAC-RH relationship in different AAE levels. Large AAC appears in the range with large AAE while
407 coarser aerosols ($\text{AAE} < 1.3$) could only be found in the condition with relatively large RH. Changes in
408 AAC with RH are different within different bins of AAE. Polynomial fitting between AAC and RH
409 indicates that the peaks of AAC mainly concentrate at the value 65% of RH for the finer ($\text{AAE} > 1.6$)
410 absorbing aerosols (unimodal). While for coarser ones, quasi-bimodal distribution of AAC is found.
411 High levels of AAC within the ranges of AAE from 1.3 to 1.6 mostly appear at the value of 40% and
412 80%. Large AACs within the ranges of AAE below 1.3 are mostly found in the value of 65% and 85%.
413 Polynomial correlation coefficients of these three fittings are 0.25, 0.16 and 0.38, respectively, which is
414 statistically significant at the confident levels of 99%, 99% and 90%.

415

416 **3.7 Aerosol absorption coefficient during pollution episodes**

417 The previous analysis indicates that extremely high levels of aerosol could be observed due to
418 serious pollution episodes, which might affect the temporal and frequency distributions of AAC in
419 urban Nanjing. Diurnal variation of BC in the period from 1st to 15th June in 2012 was altered
420 significantly from its normal distribution (Zhuang et al., 2014b), so does the AAC in this period as
421 expected. The mean value of AAC at 532 nm from January 2012 to December 2013 shown in Table 1 is
422 about 43 Mm^{-1} . However, the daily mean AACs far outstripping the value 90 Mm^{-1} , ~2 times of the
423 annual mean, could be found frequently especially in Mar, June, November in 2012 and in January,
424 November, December in 2013 (Figure 11). The largest values of the daily AAC at 532 corrected by
425 SC2006 in these months all exceeded 100 Mm^{-1} , especially on 10th June 2012 and 4th December 2013
426 on which AACs were as large as 147.19 and 149.38 Mm^{-1} , respectively. The high levels of AAC in
427 June 2012 mainly result from biomass burning in the northwestern region of Nanjing (belongs to local
428 pollution in cluster 6 of Fig. 8a), as discussed in Zhuang et al. (2014b). Levels and distributions of
429 Aerosol optical depth (AOD) from satellite (MODIS) retrievals (not shown) indicate that high aerosol
430 loadings or absorption coefficients during the periods from 9th to 13th January 2013 and from 1st to
431 8th December 2013 might possibly be caused by large scale regional pollutions over East to North
432 China (Nanjing is included). The reasons leading to high aerosol pollutions in Nanjing during the
433 sampling period would be analyzed in detailed in further studies, so does the characteristics of AAC
434 and AAE in pollution episodes.

435

436 ~~—The durations of sample spot in the filter (or the speeds of the tape advance) show significant~~

437 differences among different AAC levels as presented in Figure 12, which depicts a time series of ATN
438 for one of the seven AE 31 wavelengths, namely 520 nm. The duration of the spot is much shorter
439 (mostly no more than 5 hours) in the periods of pollution (line and markers in color) than those in clean
440 days (line and markers in grey). In the evening on 9 June 2012, the duration of the spot was only about
441 2 hours starting from 21:50 to 23:50 in the local time. Hourly mean AACs at 532 nm corrected by
442 SC2006 within this period exceeded 200 Mm^{-1} . In contrast, the new spot in the filter starting from 6:15
443 to 16:00 in the morning could last more than 9.5 hours on the 1st January in 2013 when the air quality
444 was good. The 532 nm AACs from SC2006 were mostly concentrated with the values around 30 Mm^{-1}
445 in urban Nanjing during this period.

446

447 4 Conclusions

448 In this study, the near-surface aerosol absorption coefficient (AAC) and angstrom exponent (AAE)
449 in urban Nanjing in 2012 and 2013 are investigated based on the measurements from the 7-channel
450 Aethalometer (model AE-31, Magee Scientific, USA). As suggested by Collaud Coen et al. (2010),
451 Weingartner et al. (2003) (WC2003 for short) and Schmid et al. (2006) (SC2006 for short) corrections
452 are used to assess the AAE at 660/470 nm and wavelength depended AAC. The indirect correction
453 (IDC) is also used to estimate the 532 nm-AAC based on the observed conversion factor in Nanjing.
454 Analysis in AAC is focused on at wavelength 532 nm to facilitate the comparisons between the directly
455 and indirectly correction of AACs, as the temporal variation and frequency distribution of ACC at each
456 wavelength are similar to those at 532 nm.

457 The direct and indirect corrections closely agree in terms of the temporal variation and magnitude
458 of AAC at 532 nm in the entire study period except in spring and summer possibly due to the

459 shadowing effect which is strong in these seasons. AAC at 532 nm corrected by IDC is the largest,
460 followed by that from WC2003 and SC2006. The mean AAC at 532 nm averaged from these three
461 corrections is about $43.23 \pm 28.13 \text{ Mm}^{-1}$ in urban Nanjing, with substantial seasonal and diurnal
462 variations. Higher AACs often appeared in cold seasons (at rush hours) while lower ones in summer (in
463 afternoon). Small AAC in summer (in afternoon) were partially due to large scavenging efficiency and
464 smaller emission rates of the aerosols (the well developed boundary layers). AAC in urban Nanjing is
465 much lower than that in Pearl River Delta but higher than that in non-urban sites of North China.
466 Within YRD, annual AAC in urban Nanjing is as large as that in rural areas (Lin'an). Wavelet analysis
467 suggests that variations of AAC in urban Nanjing might have cycles of 4-8 days and 9-17 days due to
468 the affection of synoptic scale (weekly) weather systems and quasi-two-week scale systems. AACs
469 follow a typical lognormal pattern in terms of the frequency distribution. For AAC at 532 nm, the range
470 from 15 to 65 Mm^{-1} dominates, accounting for more than 72% of the total data samples in the entire
471 study period. And the maximum frequencies of about 10% ~11% occur at the ranges from 25 to 30
472 Mm^{-1} . Both diurnal variations and frequency distributions of AAC shows more evident seasonality in
473 2013 than those in 2012 possibly because of the influences of the pollution episodes.

474 AAC in urban Nanjing has been affected by serious pollution episodes locally and regionally, thus
475 much enhanced AACs have been observed frequently. AACs are expected to be small in summer due to
476 low BC concentrations at the time. However, AACs were substantially large (exceeding 50 Mm^{-1}) in
477 June 2012 due to a high intensity of biomass burning around Nanjing during 1-15 June 2012.
478 Extremely high AACs in winter in 2013 might be caused by large scale regional pollutions over East to
479 North China. Hence, AAC diurnal cycle, frequency, and their seasonal variations were altered. High
480 AACs appeared at mid-night during the period 1-15 June 2012, instead of in the morning as usual.

481 Frequency of AAC followed a quasi-bimodal distribution in winter in 2013 and its values at the AAC
482 range larger than 55 Mm^{-1} were higher compared to those in other seasons in 2013. The durations of
483 sample spot in the filter (or the speeds of the tape advance) show significant differences among
484 different AAC levels. It is much shorter (mostly no more than 5 hours) in the periods of pollution than
485 those in clean days (more than 9 hours).

486 The AAC at the site generally decreases with increasing wavelength. Although AAC at 532 nm
487 from WC2003 is closed to the one from SC2006, its decline rate is smaller than SC2006's because the
488 scattering correction C from WC2003 is independent of wavelength. Thus, AAE at 660/470 nm from
489 SC2006 (=1.56) is much larger than that from WC2003 (=1.08). The scattering correction by [Schmid et al. \(2006\)](#)
490 [al. \(2006\)](#) appears more reasonable than that by [Weingartner et al. \(2003\)](#), compared to the column
491 AAE at 675/440 nm by CE-318 at the site. AAE also has strong seasonality, high in winter and low in
492 summer, possibly related to the variation in relative humidity (RH) ([Zhuang et al., 2014a](#)).

493 Wind direction shifting over different seasons might be another factor controlling the aerosol AAC
494 and AAE. Backward trajectories indicate that Nanjing could be affected by local air flow (13% ~19%)
495 and long-distance air flows mostly from northwestern, northern (>50%), eastern, southeastern and
496 southern directions. Considerable air pollutions in urban Nanjing are due to local and sub-regional
497 emissions. Air masses from the oceans and remote areas are relatively clean with low AACs. During
498 the pollution episodes in North China in 2013, a large number of aerosols was transported to Nanjing,
499 greatly enhancing AAC at the site. AAE at the site is usually low when the air masses come from the
500 oceans while it is high when the air flows from the areas of higher latitudes.

501 AAC generally increases with increasing AAE under the condition of fixed aerosol loadings in
502 urban Nanjing. The linear correlation coefficient between aerosol mass absorption coefficients (MAE)

503 at 532 nm and AAC exceeds 0.92 during the entire study period. High levels of MAC mostly appear in
504 the ranges with large AAE because the fine particles have much larger specific surface area compared
505 to coarse ones. Changes in AAE and AAC are somewhat influenced by the variations of RH. Large
506 AAEs are mostly found when the RH is low and vice versa. Changes in AAC with RH are different
507 within different bins of AAE. Unimodal and quasi-bimodal distributions of AAC vary with RH for
508 finer (AAE>1.6) and coarser (AAE<1.6) absorbing aerosols, respectively. The peak AAC mainly
509 concentrates at RH= 65% for the aerosols with AAE<1.6. For the aerosols with 1.3<AAE<1.6, the
510 maximum AACs appear around RH being 40% and 80%, while for AAE<1.3, AAC peaks around RH
511 being 65% and 85%.

512

513 **Acknowledgements:** This work was supported by the National Key Basic Research Development
514 Program of China (2014CB441203 and 2011CB403406), the Young Scientists Fund of the National
515 Natural Science Foundation of China (41205111), the New Teachers' Fund for Doctor Stations,
516 Ministry of Education (20120091120031), the Fundamental Research Funds for the Central
517 Universities (20620140744), FP7 project: REQUA (PIRSES-GA-2013-612671), and a project Funded
518 by the Priority Academic Program Development of the Jiangsu Higher Education Institutions (PAPD).
519 The authors would like to thank all members in the AERC of Nanjing University for maintaining
520 instruments. HYSPLIT model was supplied by NOAA: http://ready.arl.noaa.gov/HYSPLIT_traj.php.

521

522 **5 References**

523 Angström, A.: On the atmospheric transmission of sun radiation and on dust in the air, *Geogr. Ann.*, 11,
524 156–166, 1929.

525 Arnott, W. P., Hamasha, K., Moosmuller, H., Sheridan, P. J., and Ogren, J. A.: Towards aerosol
526 light-absorption measurements with a 7-wavelength aethalometer: evaluation with a photoacoustic
527 instrument and 3-wavelength nephelometer, *Aerosol Sci. Tech.*, 39, 17–29,
528 doi:10.1080/027868290901972, 2005.

529 Bai, H. T., Chen, Y. H., Wang, H. Q., Zhang, Q., Guo, N., Wang, S., Pan, H., and Zhang, P.: Seasonal
530 variation of aerosol optical properties at AERONET of the semi-arid region in Loess Plateau, *Arid
531 Land Geogr.*, 34, 1–8, 2011.

532 Bellouin, N., Boucher, O., Tanré, D., and Dubovik, O.: Aerosol absorption over the clear-sky oceans
533 deduced from POLDER-1 and AERONET observations, *Geophys. Res. Lett.*, 30, 1748,
534 doi:10.1029/2003GL017121, 2003.

535 Cai, H. K., Zhou, R. J., Fu, Y. F., Zheng, Y. Y., and Wang, Y. J.: Cloud-aerosol lidar with or thogonal
536 polarization detection of aerosol optical properties after a crop burning case, *Clim. Environ. Res.*,
537 16, 469–478, 2011.

538 Collaud Coen, M., Weingartner, E., Apituley, A., Ceburnis, D., Fierz-Schmidhauser, R., Flentje, H.,
539 Henzing, J. S., Jennings, S. G., Moerman, M., Petzold, A., Schmid, O., and Baltensperger, U.:
540 Minimizing light absorption measurement artifacts of the Aethalometer: evaluation of five
541 correction algorithms, *Atmos. Meas. Tech.*, 3, 457–474, doi:10.5194/amt-3-457-2010, 2010.

542 Deng, J. J., Wang, T. J., Jiang, Z. Q., Xie, M., Zhang, R. J., Huang, X. X., and Zhu, J. L.:
543 Characterization of visibility and its affecting factors over Nanjing, China, *Atmos. Res.*, 101,
544 681–691, doi:10.1016/j.atmosres.2011.04.016, 2011.

545 Forster, P., Ramaswamy, V., Artaxo, P., Berntsen, T., Betts, R., Fahey, D. W., Haywood, J., Lean, J.,
546 Lowe, D. C., Myhre, G., Nganga, J., Prinn, R., Raga, G., Schulz, M., and Van Dorland, R.: Changes

547 in atmospheric constituents and in radiative forcing, in: *Climate Change 2007: The Physical*
548 *Science Basis. Contribution of Working Group I to the Fourth Assessment Report of the*
549 *Intergovernmental Panel on Climate Change*, edited by: Solomon, S. et al., Cambridge Univ. Press,
550 Cambridge, UK, 129–234, 2007.

551 Hansen, A. D. A., Rosen, H., and Novakov, T.: The aethalometer: an instrument for the real time
552 measurements of optical absorption by aerosol particles, *Sci. Total Environ.*, 36, 191–196, 1984.

553 He, X., Li, C. C., Lau, A. K. H., Deng, Z. Z., Mao, J. T., Wang, M. H., and Liu, X. Y.: An intensive
554 study of aerosol optical properties in Beijing urban area, *Atmos. Chem. Phys.*, 9, 8903–8915,
555 doi:10.5194/acp-9-8903-2009, 2009.

556 Holler, R., Ito, K., Tohno, S., and Kasahara, M.: Wavelength-dependent aerosol single scattering albedo:
557 measurements and model calculations for a coastal site near the sea of Japan during ACE-Asia, *J.*
558 *Geophys. Res.*, 108, 8648, doi:10.1029/2002JD003250, 2003.

559 Jacobson, M. Z.: Control of fossil-fuel particulate black carbon and organic matter, possibly the most
560 effective method of slowing global warming, *J. Geophys. Res.*, 107, 4410,
561 doi:10.1029/2001JD001376, 2002.

562 Kiehl, J. T. and Briegleb, B. P.: The relative roles of sulfate aerosols and greenhouse gases in climate
563 forcing, *Science*, 260, 311–314, 1993.

564 Li, Z. Q., Lee, K. H., Wang, Y. S., Xin, J. Y., and Hao, W. M.: First observation-based estimates of
565 cloud-free aerosol radiative forcing across China, *J. Geophys. Res.*, 115, D00K18,
566 doi:10.1029/2009JD013306, 2010.

567 Liao, H. and Seinfeld, J. H.: Global impacts of gas-phase chemistry-aerosol interactions on direct
568 radiative forcing by anthropogenic aerosols and ozone, *J. Geophys. Res.*, 110, D18208,

569 doi:10.1029/2005JD005907, 2005.

570 Menon, S., Hansen, J., Nazarenko, L., and Luo, Y. F.: Climate effects of black carbon aerosols in China
571 and India, *Science*, 297, 2250–2253, doi:10.1126/science.1075159, 2002.

572 Penner, J. E., Andreae, M., Annegarn, H., Barrie, L., Feichter, J., Hegg, D., Jayaraman, A., Leaitch, R.,
573 Murphy, D., Nganga, J., and Pitari, G.: Aerosols, their direct and indirect effects, in: *Climate*
574 *Change 2001: The Scientific Basis. Contribution of Working Group I to the Third Assessment*
575 *Report of the Intergovernmental Panel on Climate Change*, edited by: Houghton, J. T. et al.,
576 Cambridge University Press, Cambridge, UK and New York, NY, USA, 289–348, 2001.

577 Petzold, A., Kopp, C., and Niessner, R.: The dependence of the specific attenuation cross-section on
578 black carbon mass fraction and particle size, *Atmos. Environ.*, 31, 661–672, 1997.

579 Schmid, O., Artaxo, P., Arnott, W. P., Chand, D., Gatti, L. V., Frank, G. P., Hoffer, A., Schnaiter, M., and
580 Andreae, M. O.: Spectral light absorption by ambient aerosols influenced by biomass burning in the
581 Amazon Basin. I: Comparison and field calibration of absorption measurement techniques, *Atmos.*
582 *Chem. Phys.*, 6, 3443–3462, doi:10.5194/acp-6-3443-2006, 2006.

583 Streets, D. G., Gupta, S., Waldhoff, S. T., Wang, M. Q., Bond, T. C., and Bo, Y. Y.: Black carbon
584 emissions in China, *Atmos. Environ.*, 35, 4281–4296, doi:10.1016/S1352-2310(01)00179-0, 2001.

585 Virkkula, A., Makela, T., Hillamo, R., Yli-Tuomi, T., Hirsikko, A., Hameri, K., and Koponen, I. K.: A
586 simple procedure for correcting loading effects of aethalometer data, *J. Air Waste Manage.*, 57,
587 1214–1222, doi:10.3155/1047-3289.57.10.1214, 2007.

588 Wang, Y., Che, H. Z., Ma, J. Z., Wang, Q., Shi, G. Y., Chen, H. B., Goloub, P., and Hao, X. J.: Aerosol
589 radiative forcing under clear, hazy, foggy, and dusty weather conditions over Beijing, China,
590 *Geophys. Res. Lett.*, 36, L06804, doi:10.1029/2009GL037181, 2009.

591 Weingartner, E., Saathoff, H., Schnaiter, M., Streit, N., Bitnar, B., and Baltensperger, U.: Absorption of
592 light by soot particles: determination of the absorption coefficient by means of aethalometers, *J.*
593 *Aerosol Sci.*, 34, 1445–1463, doi:10.1016/S0021-8502(03)00359-8, 2003.

594 Wu, D., Mao, J. T., Deng, X. J., Tie, X. X., Zhang, Y. H., Zeng, L. M., Li, F., Tan, H. B., Bi, X. Y.,
595 Huang, X. Y., Chen, J., and Deng, T.: Black carbon aerosols and their radiative properties in the
596 Pearl River Delta region, *Sci. China Ser. D*, 52, 1152–1163, doi:10.1007/s11430-009-0115-y, 2009.

597 Wu, D., Wu, C., Liao, B., Chen, H., Wu, M., Li, F., Tan, H., Deng, T., Li, H., Jiang, D., and Yu, J. Z.:
598 Black carbon over the South China Sea and in various continental locations in South China, *Atmos.*
599 *Chem. Phys.*, 13, 12257–12270, doi:10.5194/acp-13-12257-2013, 2013.

600 Wu, Y. F., Zhang, R. J., Pu, Y. F., Zhang, L. M., Ho, K. F., and Fu, C. B.: Aerosol optical properties
601 observed at a semi-arid rural site in northeastern China, *Aerosol Air Qual. Res.*, 12, 503–514, 2012.

602 Xia, X. A., Li, Z. Q., Holben, B., Wang, P., Eck, T., Chen, H. B., Cribb, M., and Zhao, Y. X.: Aerosol
603 optical properties and radiative effects in the Yangtze Delta region of China, *J. Geophys. Res.*, 112,
604 D22S12, doi:10.1029/2007JD008859, 2007.

605 Xiao, Z. Y., Jiang, H., Chen, J., Wang, B., and Jiang, Z. S.: Monitoring the aerosol optical properties
606 over Hangzhou using remote sensing data, *Acta Sci. Circumst.*, 31, 1758–1767, 2011.

607 Xu, J., Bergin, M. H., Greenwald, R., Schauer, J. J., Shafer, M. M., Jaffrezo, J. L., and Aymoz, G.:
608 Aerosol chemical, physical, and radiative characteristics near a desert source region of Northwest
609 China during ACE-Asia, *J. Geophys. Res.*, 109, D19S03, doi:10.1029/2003JD004239, 2004.

610 Yan, P.: Study on the aerosol optical properties in the background regions in the East part of China,
611 PhD Thesis, Peking University, China, 2006.

612 Yan, P., Tang, J., Huang, J., Mao, J. T., Zhou, X.J., Liu, Q., Wang, Z. F., and Zhou, H. G.: The

613 measurement of aerosol optical properties at a rural site in Northern China, *Atmos. Chem. Phys.*, 8,
614 2229–2242, doi:10.5194/acp-8-2229-2008, 2008.

615 Zhang, Q., Streets, D. G., Carmichael, G. R., He, K. B., Huo, H., Kannari, A., Klimont, Z., Park, I. S.,
616 Reddy, S., Fu, J. S., Chen, D., Duan, L., Lei, Y., Wang, L. T., and Yao, Z. L.: Asian emissions in
617 2006 for the NASA INTEX-B mission, *Atmos. Chem. Phys.*, 9, 5131–5153,
618 doi:10.5194/acp-9-5131-2009, 2009.

619 Zhou, B., Zhang, L., Cao, X. J., Han, X., Zhang, W., and Feng, G. H.: Analyses on atmospheric aerosol
620 optical properties with lidar data in Lanzhou suburb, *Plateau Meteorol.*, 30, 1011–1017, 2011.

621 Zhu, J., Wang, T., Talbot, R., Mao, H., Hall, C. B., Yang, X., Fu, C., Zhuang, B., Li, S., Han, Y., and
622 Huang, X.: Characteristics of atmospheric Total Gaseous Mercury (TGM) observed in urban
623 Nanjing, China, *Atmos. Chem. Phys.*, 12, 12103–12118, doi:10.5194/acp-12-12103-2012, 2012.

624 Zhuang, B. L., Li, S., Wang, T. J., Deng, J. J., Xie, M., Yin, C. Q., and Zhu, J. L.: Direct radiative
625 forcing and climate effects of anthropogenic aerosols with different mixing states over China,
626 *Atmos. Environ.*, 79, 349–361, doi:10.1016/j.atmosenv.2013.07.004, 2013a.

627 Zhuang, B. L., Liu, Q., Wang, T. J., Yin, C. Q., Li, S., Xie, M., Jiang, F., and Mao, H. T.: Investigation
628 on semi-direct and indirect climate effects of fossil fuel black carbon aerosol over China, *Theor.*
629 *Appl. Climatol.*, 114, 651–672, doi:10.1007/s00704-013-0862-8, 2013b.

630 Zhuang, B. L., Wang, T. J., Li, S., Liu, J., Talbot, R., Mao, H. T., Yang, X. Q., Fu, C. B., Yin, C. Q.,
631 Zhu, J. L., Che, H. Z., and Zhang, X. Y.: Optical properties and radiative forcing of urban aerosols
632 in Nanjing, China, *Atmos. Environ.*, 83, 43–52, 2014a.

633 Zhuang, B. L., Wang, T. J., Liu, J., Li, S., Xie, M., Yang, X. Q., Fu, C. B., Sun, J. N., Yin, C. Q., Liao, J.
634 B., Zhu, J. L., and Zhang, Y.: Continuous measurement of black carbon aerosol in urban Nanjing of

635 Yangtze River Delta, China, Atmos. Environ., 89, 415–424, 2014b.

636

637 **Figure captions:**

638 Figure 1. Double logarithmic plot of C versus λ for $\alpha_a=1$ (orange), 1.5 (green), 2 (blue) and 2.5
639 (violet), respectively.

640 Figure 2. Variations of the coefficients A and B with α_a .

641 Figure 3. Monthly variations of the aerosol absorption coefficients (Mm^{-1}) at 532 nm in urban Nanjing
642 in 2012 (a) and 2013 (b). The 10th, 25th, median, 75th, 90th percentile values of the coefficient
643 corrected by SC2006 are presented as box plot. The monthly means of the coefficients corrected by
644 indirect way (red), WC2003 (blue) and SC2006 (light green) are presented as line-markers.

645 Figure 4. Diurnal variations of the aerosol absorption coefficients at 532 nm in urban Nanjing. (a) the
646 two-year (2012-2013) coefficients corrected by indirect way (red), WC2003 (blue) and SC2006 (light
647 green) and (b) the coefficients corrected by SC2006 in separate seasons of 2012 and 2013. Mar, April
648 and May represent the spring, June, July and August represent the summer, September, October and
649 November represent the fall, and January, February and December in 2012 (2013) represent the winter
650 in 2012 (2013).

651 Figure 5. Frequency distributions of the aerosol absorption coefficients at 532 nm in urban Nanjing. (a)
652 the two-year (2012-2013) coefficients corrected by indirect way (red), WC2003 (blue) and SC2006
653 (light green), (b) the coefficients corrected by SC2006 in separate year 2012 (solid bar) and 2013 (erase
654 bar), and (c) the coefficients corrected by SC2006 in separate seasons of separate year.

655 Figure 6. The local wavelet power spectrum (a) and wavelet real part spectrum (b) of the aerosol
656 absorption coefficient at 532 nm using the Morlet wavelet. The left axis is the wavelet scale (in day)

657 corresponding to the Fourier period on the right axis. The bottom axis is local time (month). The filled
658 parts in Fig. 6a indicate passing 95% confidence level test, and the parts below the dashed line are
659 unlikelihood.

660 Figure 7. Dependence of the aerosol absorption coefficient corrected by WC2003 (blue) and SC2006
661 (green) on the wavelength in urban Nanjing during the period from 2012 to 2013 (Fig. a). Annual (dash
662 lines) and seasonal (bars with error bar) absorption angstrom exponents at 660/470 nm from WC2003
663 (light blue) and SC2006 (green) both in 2012 (Fig. b) and 2013 (Fig. c).

664 Figure 8. Clusters of 96-h back trajectories arriving at the study site at 100 m in 2012 (a) and 2013 (b)
665 simulated by HYSPLIT model and the probability distributions of 6 hours interval near surface wind
666 speed in different wind directions in Nanjing (c).

667 Figure 9. The 10%, 25%, 50%, 75% and 90% percentile values of the aerosol absorption coefficient (a,
668 b) and absorption angstrom exponent (c, d) in each cluster of back trajectories in 2012 (Fig. 8a) and
669 2013 (Fig. 8b).

670 Figure 10. Relationships between the aerosol mass (or specific) absorption coefficient (m^2/g) and its
671 angstrom exponent (a, scatter plots) and the effects of relative humidity on the aerosol absorption
672 coefficient (a, in color and b) in different absorption angstrom exponent levels.

673 Figure 11. Time series of daily mean aerosol absorption coefficient at 532 nm corrected by IDC (red),
674 WC2003 (blue) and SC2006 (green) in the period from 2012 to 2013.

675 ~~Figure 12. Time series of the light attenuation at 520 nm in different pollution episodes (colors) and in~~
676 ~~clean day (grey). The time interval between two markers is 15 minutes.~~

677

678

679
680
681
682
683
684
685
686
687
688
689
690
691
692
693
694

695 **Tables:**

696 Table 1. Statistical values of annual aerosol absorption coefficient (Mm^{-1}) and absorption angstrom
697 exponent in urban Nanjing

Year	Schemes	All wave AAC		Visible wave AAC		532 nm- AAC		AAE (660/470 nm)	
		Average	Std	Average	Std	Average	Std	Average	Std
2012	IDC	/	/	/	/	42.99	26.55	/	/

	SC2006	39.70	35.26	40.34	27.10	41.02	25.70	1.58	0.20
	WC2003	40.48	31.26	41.97	27.29	42.44	26.59	1.09	0.20
2013	IDC	/	/	/	/	45.81	30.22	/	/
	SC2006	41.91	38.64	42.66	30.61	42.87	29.14	1.54	0.25
	WC2003	42.39	34.41	43.99	30.79	44.34	30.15	1.07	0.21
2-year	IDC	/	/	/	/	44.38	28.45	/	/
period	SC2006	40.78	36.97	41.47	28.89	41.93	27.47	1.56	0.23
	WC2003	41.41	32.86	42.97	29.08	43.38	28.41	1.08	0.20

698 IDC: The coefficients from the indirect correction.

699 SC2006: The coefficients corrected by [Schmid et al. \(2006\)](#).

700 WC2003: The coefficients corrected by [Weingartner et al. \(2003\)](#).

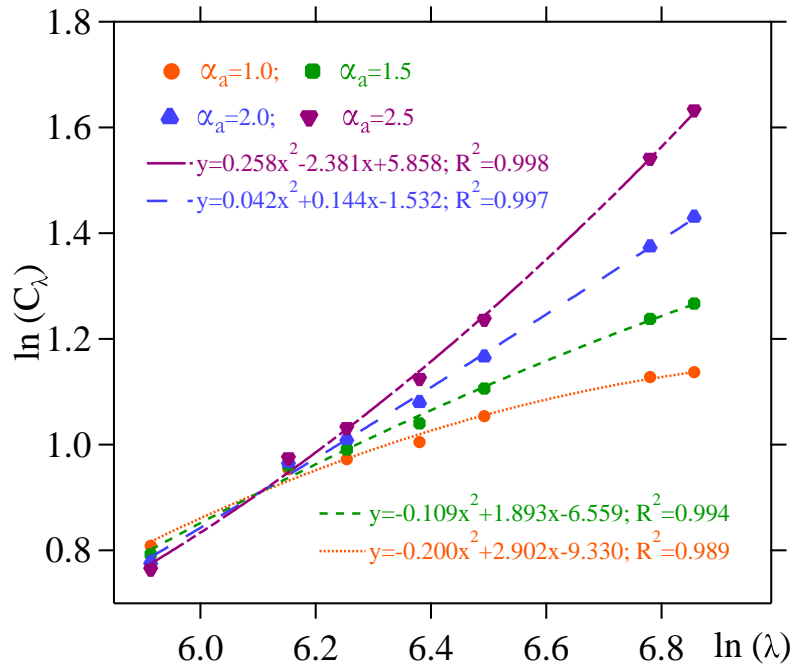
701 AAC: Aerosol absorption coefficients.

702 AAE: Absorption angstrom exponent.

703

704

705 **Figures:**

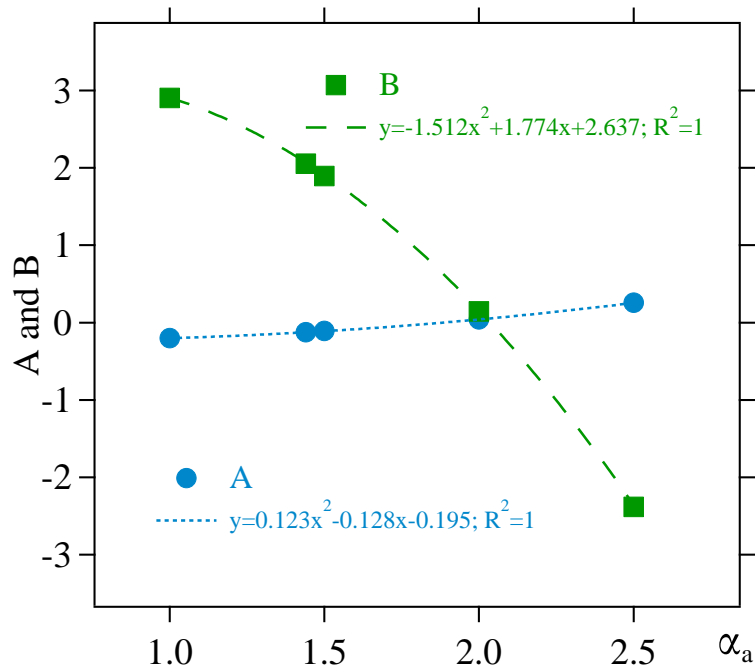


706

707

Figure 1.

708



709

710

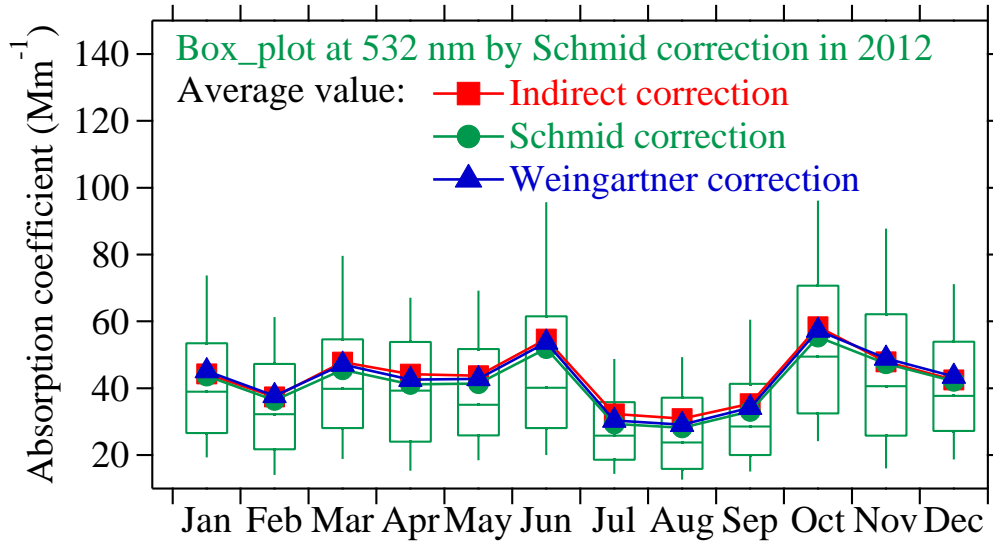
Figure 2.

711

712

713

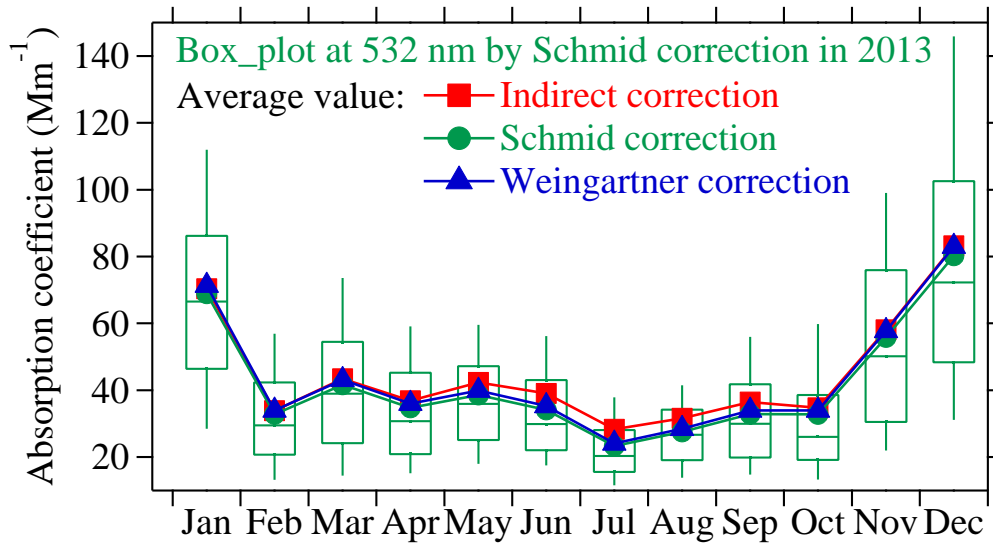
714



715

716

a)



717

718

b)

Figure 3

719

720

721

722

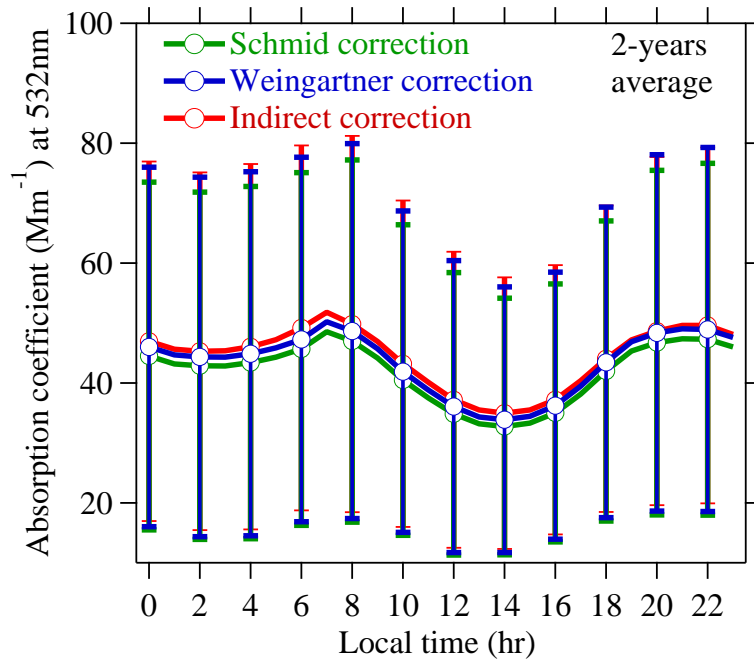
723

724

725

726

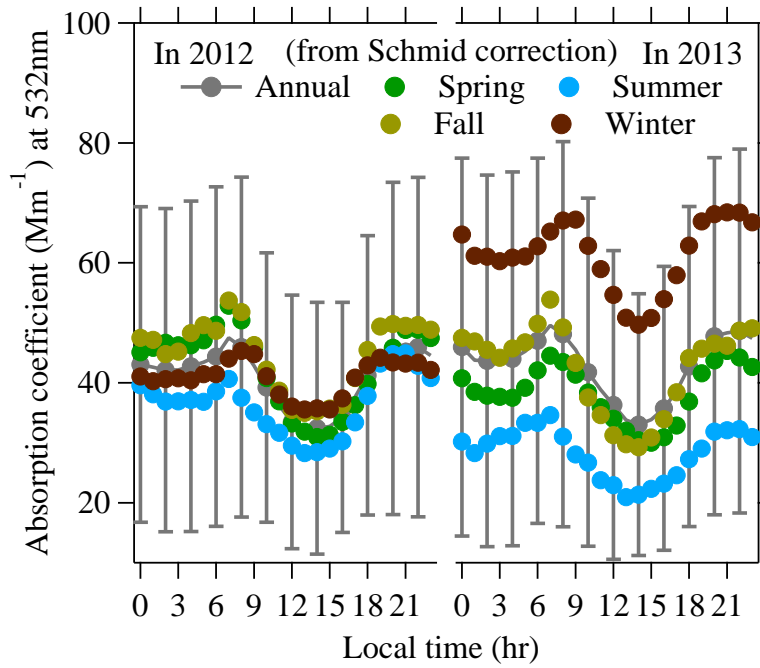
727



728

729

a)



730

731

732

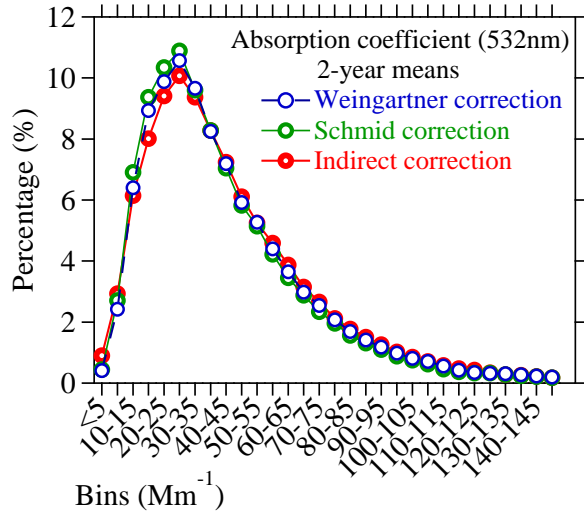
733

734

735

b)

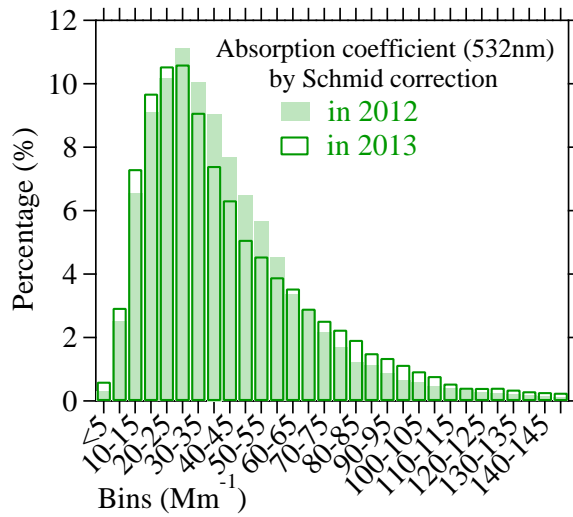
Figure 4



736

737

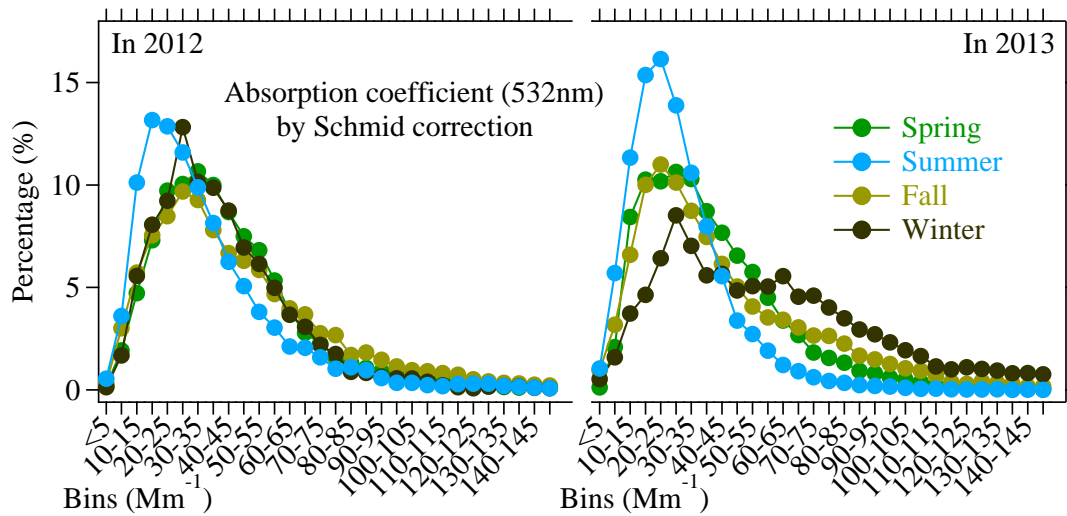
a)



738

739

b)



740

741

c)

742

Figure 5

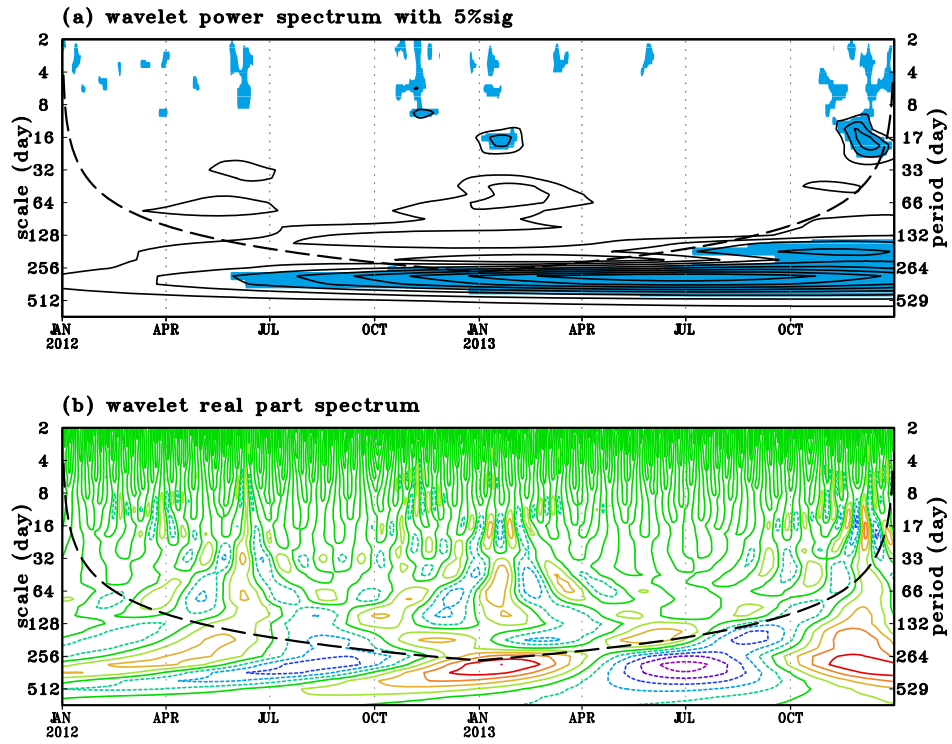


Figure 6

743

744

745

746

747

748

749

750

751

752

753

754

755

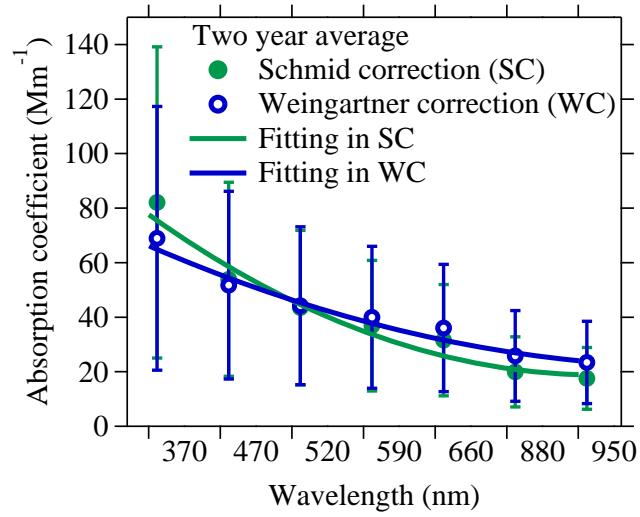
756

757

758

759

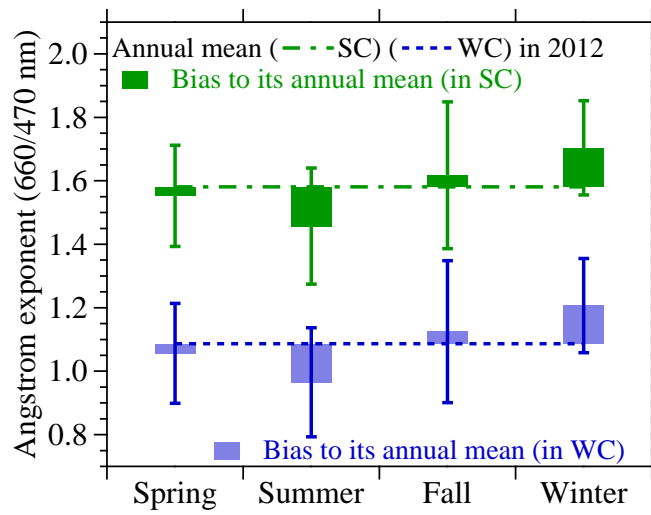
760



761

762

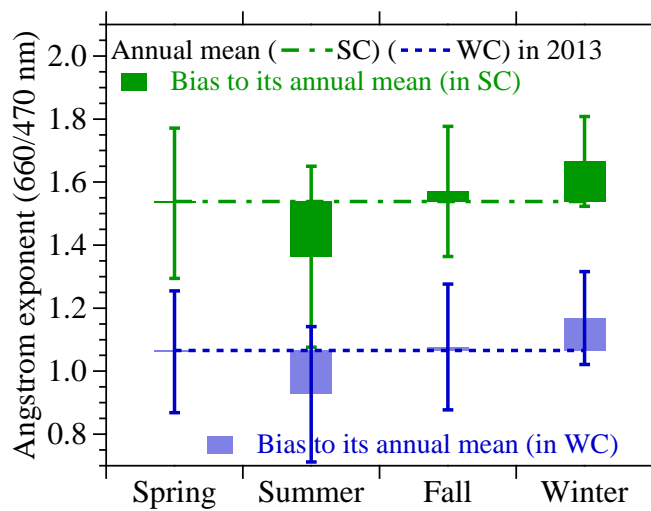
a)



763

764

b)



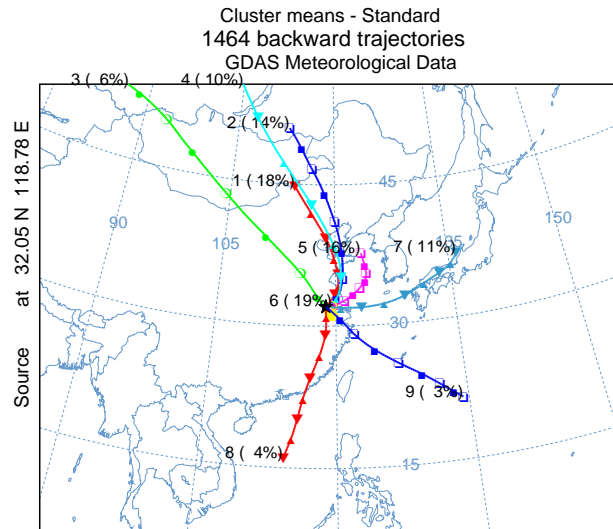
765

766

767

c)

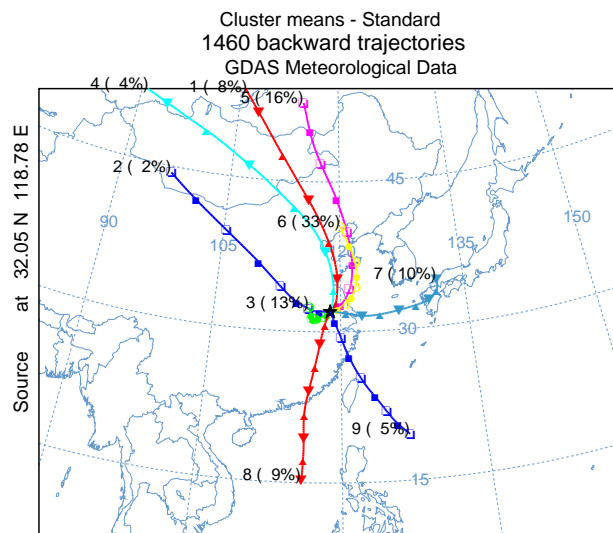
Figure 7



768

769

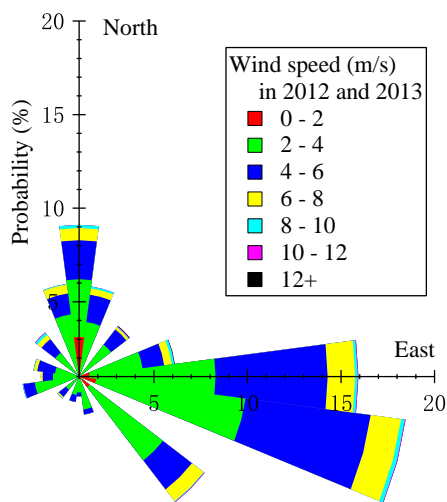
a)



770

771

b)



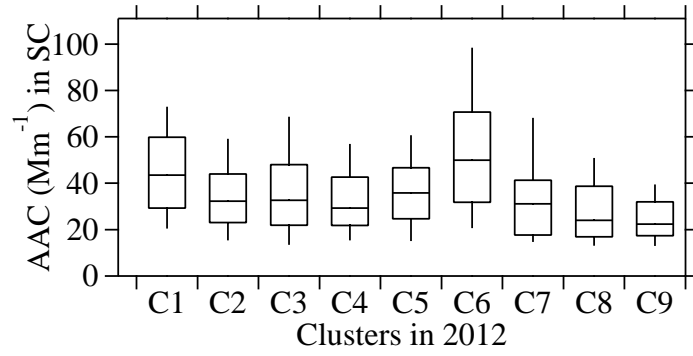
772

773

774

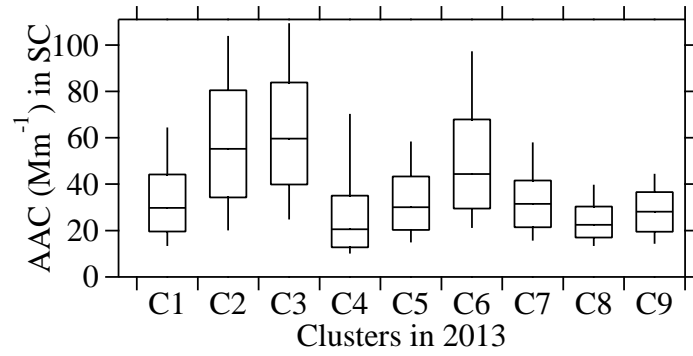
c)

Figure 8



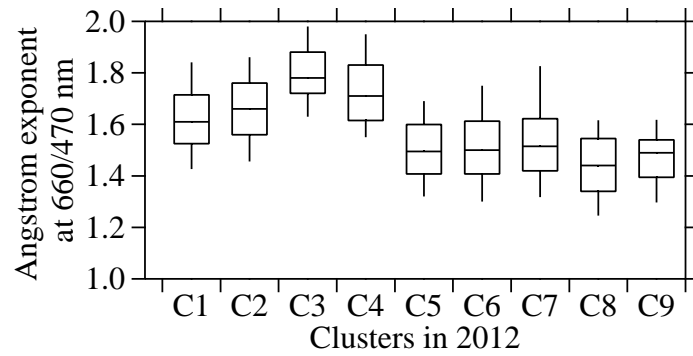
775
776

a)



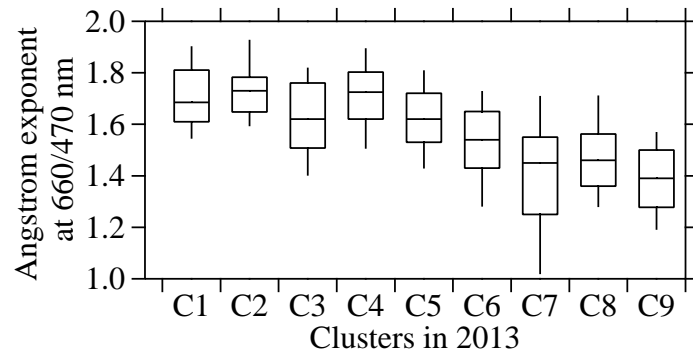
777
778

b)



779
780

c)

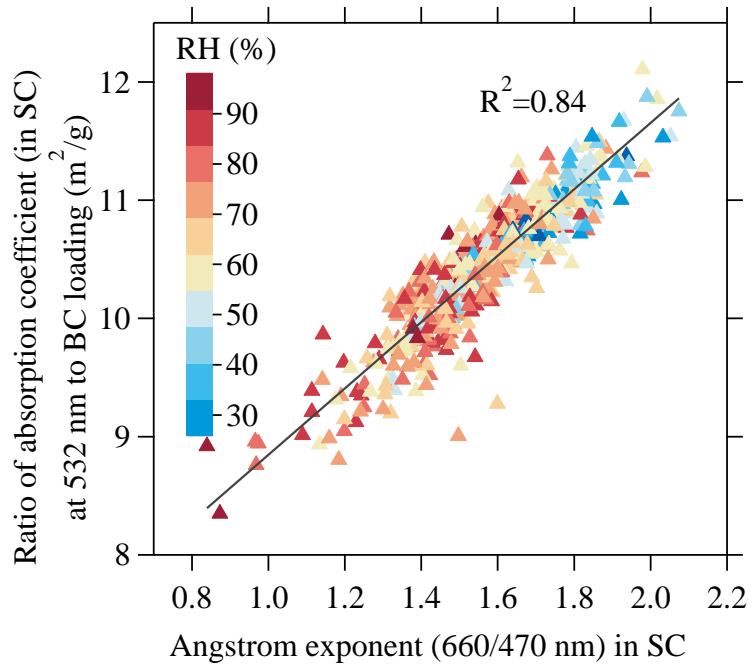


781
782

d)

783
784

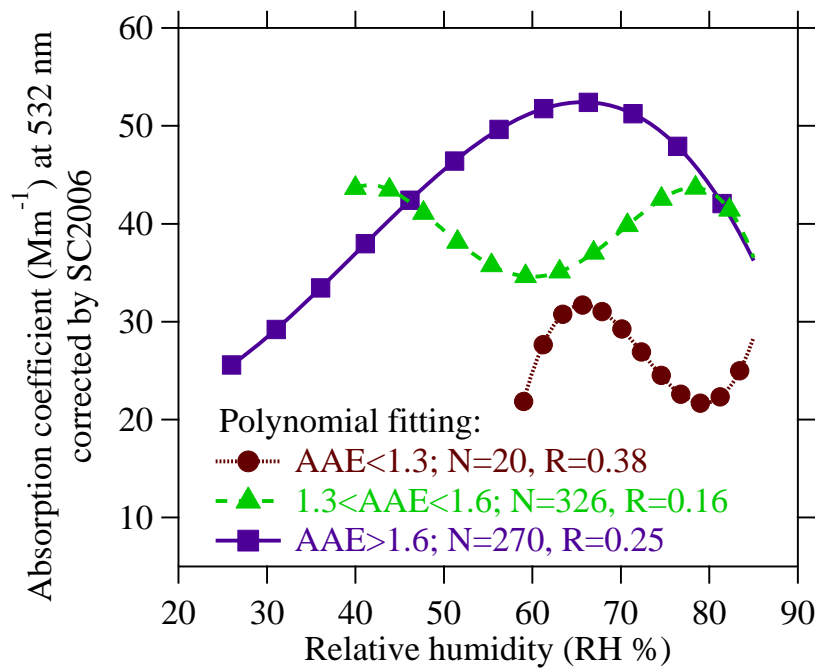
Figure 9



785

786

a)



787

788

789

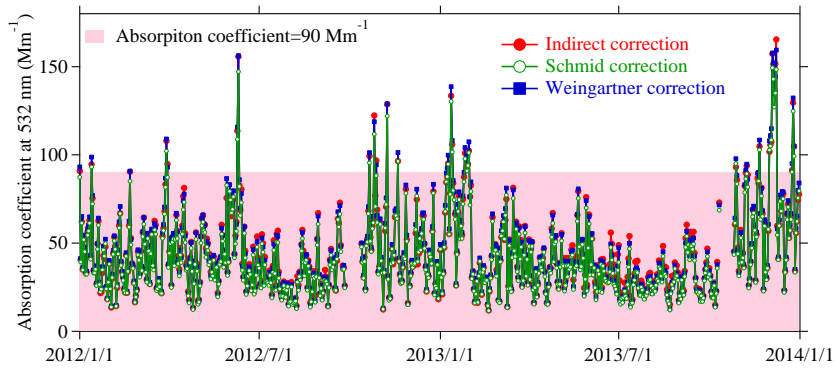
790

791

792

793

Figure 10

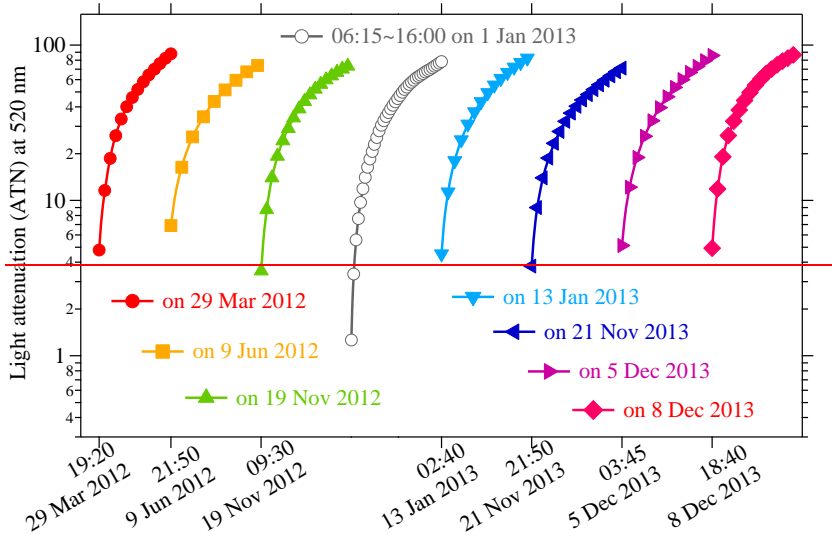


794

795

796

Figure 11



797

798

799

Figure 12